Tran-SET

Transportation Consortium of South-Central States

Solving Emerging Transportation Resiliency, Sustainability, and Economic Challenges through the Use of Innovative Materials and Construction Methods: From Research to Implementation

Smart Battery Management System for Electric Vehicles: Self-learning Algorithms for Simultaneous State and Parameter Estimation, and Stress Detection

Project No. 20ITSOSU38

Lead University: Oklahoma State University

Final Report

December 2021

Disclaimer

The contents of this report reflect the views of the authors, who are responsible for the facts and the accuracy of the information presented herein. This document is disseminated in the interest of information exchange. The report is funded, partially or entirely, by a grant from the U.S. Department of Transportation's University Transportation Centers Program. However, the U.S. Government assumes no liability for the contents or use thereof.

Acknowledgements

This work was supported by U.S. Department of Transportation, Transportation Consortium of South-Central States (Tran-SET). The authors would like to cordially thank the Dean Research and the Head, Division of Engineering Technology, College of Engineering, Architecture and Technology, Oklahoma State University, for the financial support to procure test equipment. The authors would also like to thank Dr. Hao Xu from University of Nevada Reno, Dr. Umamaheswar Rao Tida from University of North Dakota, and Dr. Huaxia Wang, from Oklahoma State University for their support and inputs as the program review committee.

TECHNICAL DOCUMENTATION PAGE

1. Project No.	2. Government Accession No.	3. Recipient's Catalog No.
20ITSOSU38		

4. Title and Subtitle	5. Report Date
Smart Battery Management System for Electric Vehicles: Self-learning Algorithms for Simultaneous State and Parameter Estimation, and Stress Detection	Dec. 01, 2021
	6. Performing Organization Code
7. Author(s)	**8. Performing Organization Report No.**
Avimanyu Sahoo Samir Ahmed	
9. Performing Organization Name and Address	**10. Work Unit No. (TRAIS)**
Transportation Consortium of South-Central States (Tran-SET) University Transportation Center for Region 6 3319 Patrick F. Taylor Hall, Louisiana State University, Baton Rouge, LA 70803	**11. Contract or Grant No.** 69A3551747106
12. Sponsoring Agency Name and Address	**13. Type of Report and Period Covered**
United States of America Department of Transportation Research and Innovative Technology Administration	Final Research Report Aug. 2020 – Aug. 2021
	14. Sponsoring Agency Code

15. Supplementary Notes

Report uploaded and accessible at Tran-SET's website (http://transet.lsu.edu/).

16. Abstract

The project proposes to develop parameter-varying SOH-coupled models for lithium-ion battery and self-learning algorithms to learn the model for simultaneous state and parameter estimation and fault detection. The traditional battery models use constant parameters, limiting their accuracy for predicting the state of the charge and health over the complete life-cycle. In practice, the battery parameters vary with the change in the state of charge and state of health. SOH-coupled models can be used to estimate the state of charge and health accurately. Further, obtaining the model parameters is also a challenging task for designing filters or observers for state estimation. A self-learning algorithm can eliminate the requirement of the model parameters. In this project, three SOH-coupled models are proposed and validated experimentally. The models are also used to design extended Kalman filters (EKF) for the state of charge, state of health, core and surface temperature, and internal resistance estimation. The results showed that the SOH-coupled models are more effective when compared to the uncoupled models in the literature. Further, it was found that EKFs based state estimation errors were within 1%. The self-learning algorithm using a two-layer neural network showed the ability to learn the models in real-time. However, the state estimation errors are higher for the self-learning scheme compared to the EKF based approaches. This is due to the limited measurement and online training schemes utilized to train neural networks. This requires further investigation in hyper-parameter tuning for implementation. Finally, a model-based fault detection scheme was proposed to detect internal thermal fault at its onset. The SOH-coupled model is reformulated to incorporate the internal resistance as a state. The EKF is used as a fault detection observer. The proposed fault detection scheme is validated using numerical simulation. It was observed that the fault detection scheme with SOH coupled electro-thermal-aging model could effectively detect a thermal fault at its incipient state.

17. Key Words	18. Distribution Statement
Lithium-ion battery management system, internal and external degradation, state of charge and state of health, Lithium-ion battery modeling, fault detection.	No restrictions. This document is available through the National Technical Information Service, Springfield, VA 22161.

19. Security Classif. (of this report)	20. Security Classif. (of this page)	21. No. of Pages	22. Price
Unclassified	Unclassified	52	

Form DOT F 1700.7 (8-72) **Reproduction of completed page authorized.**

SI* (MODERN METRIC) CONVERSION FACTORS

APPROXIMATE CONVERSIONS TO SI UNITS

Symbol	When You Know	Multiply By	To Find	Symbol
		LENGTH		
in	inches	25.4	millimeters	mm
ft	feet	0.305	meters	m
yd	yards	0.914	meters	m
mi	miles	1.61	kilometers	km
		AREA		
in^2	square inches	645.2	square millimeters	mm^2
ft^2	square feet	0.093	square meters	m^2
yd^2	square yard	0.836	square meters	m^2
ac	acres	0.405	hectares	ha
mi^2	square miles	2.59	square kilometers	km^2
		VOLUME		
fl oz	fluid ounces	29.57	milliliters	mL
gal	gallons	3.785	liters	L
ft^3	cubic feet	0.028	cubic meters	m^3
yd^3	cubic yards	0.765	cubic meters	m^3
		NOTE: volumes greater than 1000 L shall be shown in m^3		
		MASS		
oz	ounces	28.35	grams	g
lb	pounds	0.454	kilograms	kg
T	short tons (2000 lb)	0.907	megagrams (or "metric ton")	Mg (or "t")
		TEMPERATURE (exact degrees)		
^oF	Fahrenheit	5 (F-32)/9 or (F-32)/1.8	Celsius	^oC
		ILLUMINATION		
fc	foot-candles	10.76	lux	lx
fl	foot-Lamberts	3.426	$candela/m^2$	cd/m^2
		FORCE and PRESSURE or STRESS		
lbf	poundforce	4.45	newtons	N
lbf/in^2	poundforce per square inch	6.89	kilopascals	kPa

APPROXIMATE CONVERSIONS FROM SI UNITS

Symbol	When You Know	Multiply By	To Find	Symbol
		LENGTH		
mm	millimeters	0.039	inches	in
m	meters	3.28	feet	ft
m	meters	1.09	yards	yd
km	kilometers	0.621	miles	mi
		AREA		
mm^2	square millimeters	0.0016	square inches	in^2
m^2	square meters	10.764	square feet	ft^2
m^2	square meters	1.195	square yards	yd^2
ha	hectares	2.47	acres	ac
km^2	square kilometers	0.386	square miles	mi^2
		VOLUME		
mL	milliliters	0.034	fluid ounces	fl oz
L	liters	0.264	gallons	gal
m^3	cubic meters	35.314	cubic feet	ft^3
m^3	cubic meters	1.307	cubic yards	yd^3
		MASS		
g	grams	0.035	ounces	oz
kg	kilograms	2.202	pounds	lb
Mg (or "t")	megagrams (or "metric ton")	1.103	short tons (2000 lb)	T
		TEMPERATURE (exact degrees)		
^oC	Celsius	1.8C+32	Fahrenheit	^oF
		ILLUMINATION		
lx	lux	0.0929	foot-candles	fc
cd/m^2	$candela/m^2$	0.2919	foot-Lamberts	fl
		FORCE and PRESSURE or STRESS		
N	newtons	0.225	poundforce	lbf
kPa	kilopascals	0.145	poundforce per square inch	lbf/in^2

TABLE OF CONTENTS

LIST OF FIGURES

LIST OF TABLES

ACRONYMS, ABBREVIATIONS, AND SYMBOLS

BMS	Battery management system
CC	Constant Current
CEI	Cathode electrolyte interface,
CV	Constant voltage
DOD	Depth of discharge
ECM	Equivalent circuit model
EKF	Extended Kalman filter
EV	Electric vehicle
LAM	Loss of active material
LIBs	Lithium-ion batteries
Li-ion	Lithium-ion
LLI	Loss of lithium-ions
NN	Neural network
PDE	Partial differential equation
SEI	Solid-electrolyte interface
SMO	Sliding mode observer
SOC	State of charge
SOH	State of health

EXECUTIVE SUMMARY

Electric vehicles (EVs) are the future means of transportation systems due to their cost-effective and environment-friendly nature. The rapid advancement in energy storage technologies such as lithium-ion (Li-ion) batteries with high energy density has accelerated the acceptance of EVs in recent years. Efficient and safe operation of Li-ion batteries in EVs requires an intelligent and smart battery management system (BMS) capable of learning the health degradation in real-time for accurately estimating the state-of-charge (SOC) and the state-of-health (SOH). This will add autonomy to the BMS in health-conscious decision-making, such as fast charging, discharging, cell balancing, and optimal power and energy management. Therefore, the project's main objective is to develop intelligent BMS algorithms by 1) introducing enhanced SOH-coupled parameter-varying dynamical model of Li-ion battery and 2) real-time learning algorithms to learn the parameter-varying model. The enhanced model of the Li-ion battery can be employed for internal faults and stress detection by incorporating the SOH indicators, such as capacity loss and power loss under normal and accelerated degradation conditions. The research is categorized under four main technical tasks to achieve this overall objective.

In the first task, we have conducted an in-depth literature review to investigate various internal and external stress-inducing factors on Li-ion batteries used onboard EVs. Our goal was to study the effects of internal and external degradation inducing factors on the capacity fade, power fade, and internal parameter variation. The survey focused on four aspects of the life cycle of the Li-ion battery: a) internal degradation mechanisms and their modeling, b) external factors affecting the degradation of the battery, c) advanced and recent SOH estimation methods. We have reviewed 179 journal and conference papers and compiled the recent results in tabular forms for quick reference along with discussion and conclusions. We systematically presented the evolution of chemical and mechanical degradation due to solid-electrolyte interface (SEI) layer formation, fracture, lithium plating, dendrite formation, and their mathematical modeling. The inter-relations among these degradation mechanisms and their effects on capacity and power fade are also discussed. It can be concluded from the review that while the fracture, lithium plating, and dendrite formation lead to loss of active lithium resulting in capacity loss, the SEI layer formation affects both the capacity loss and power fade.

In the second task, our goal was to develop an enhanced SOC and SOH-dependent parameter varying ECM of Li-ion batteries by accounting for normal and accelerated aging in extreme conditions. Based on our literature review, the existing electro-thermal-aging models of the LIB were not coupled with changes in the capacity fade. To bridge the gap and for a more accurate SOH estimation, we have proposed three SOH coupled models of lithium-ion batteries. Each model is an improved version of the previous model and developed to perform specific tasks. The models integrate the electric, thermal, and health characteristics of the battery. The proposed Model 1 incorporates the change in the battery's usable capacity due to SOH decay (capacity fade) while estimating the SOC. It improves model accuracy since the ECM parameters are dependent on SOC and SOH. Model 2 incorporates the nonlinear output voltage equation as part of the dynamics such that this model can be learned using a single neural network (NN). Finally, Model 2 is improved further by incorporating the dynamics of the internal parameter (ohmic resistance). This allows estimating the SOH (capacity face), SOC, and the internal resistance, simultaneously. The changes in internal resistance provide information about the second SOH indicator (power fade) and can be used for fault and stress detection. We have conducted numerical and experimental validation of these models using the 26650 cylindrical Li-ion battery.

In the third task, we have developed self-learning algorithms using neural networks to learn the SOC and SOH-dependent battery model developed in Task 2 with real-time measurements. We employed a two-layer NN to learn the Model 2 of the lithium-ion battery. The input layer NN weights are initialized randomly, and the output layer weights are trained online using the real-time measurements from the battery. We also carried out analytical convergence analysis for the NN weight estimation errors using Lyapunov-based stability approaches. The NN approximation errors are found to be higher than the conventional Kalman filter-based approaches. This is due to the limited number of measurements (voltage, current, and temperature) to learn the higher dimensional model. In the fourth and final task, we developed faults/stress detection schemes using the developed Model 3. Due to the higher approximation error with NN-based learning, we employed a Kalman filter-based approach to estimate the states and detect the internal fault of the battery. The Kalman filter estimated the core and surface temperature along with the internal parameter (resistance). We introduced a thermal fault during the simulation and monitored the terminal voltage of the battery for detection. The fault detection residual is generated by comparing the output of the faulted model and the Kalman filter. A detection threshold is used based on expert knowledge to detect the fault.

In summary, three novel SOH coupled electro-thermal-aging models for smart BMS of Li-ion battery are developed and validated both numerically and experimentally. Extended Kalman filter and NN-based self-learning approaches are developed and employed to estimate the battery's SOC, SOH, and parameter. The results showed that the developed models outperformed the existing ones and can be utilized for SOH, SOC, and parameter estimation. The project also introduced self-learning algorithms to learn the models from real-time measurements. The approximation error in the NN-based self-learning algorithm is found to be higher when compared to the extended Kalman filter-based approach. It, therefore, needs further investigation to tune the hyperparameters of the online neural network weight training scheme. Further experimental evaluation and field tests are required for implementing these algorithms onboard BMS of the EVs.

1. INTRODUCTION

Electric vehicles (EVs) are the future transportation systems due to their cost-effective and environment-friendly nature. The rapid advancement in energy storage technologies, such as lithium-ion batteries (LIBs), with high energy density, has accelerated the acceptance of EVs in recent years. In 2018, the United States of America witnessed the highest growth rate in the adoption of EVs. An increase of 81 percent in sales of EVs has been seen in the year 2018 compared to 2017, i.e., approximately 360,000 plug-in EVs were sold in 2018 *(1)*. In addition, the Federal Highway Administration (FHWA) recently established the EV charging corridors, spanning over 35 states *(2)*. Several automotive industries have also proposed their future road map to meet the anticipated demand of 44 million EVs by the end of 2030 *(3)*.

The recent additions of LIBs in the high-end plug-in EV categories offer a range of approximately 300 miles on a single full charge. It is expected that the LIB market will also reach $92 billion by 2024 *(4)*. However, the volatility of internal constituents, flammability, and toxicity of the electrolyte, which is the flip side of the high energy density of LIB, make the cells thermally unstable at high temperatures and reduce life when operating at low temperatures. Further, the low tolerance to abuse (overcharging and discharging) and vulnerability to thermal runway and explosion jeopardize user safety *(5)*, which is a national concern. Therefore, a battery management system (BMS) *(6)* is employed for the safe and efficient operation of the LIB, as shown in Figure 1. In addition to battery operation, the BMS also estimates the state of the charge (SOC) using a dynamical model of the battery, which is utilized to compute the EV range.

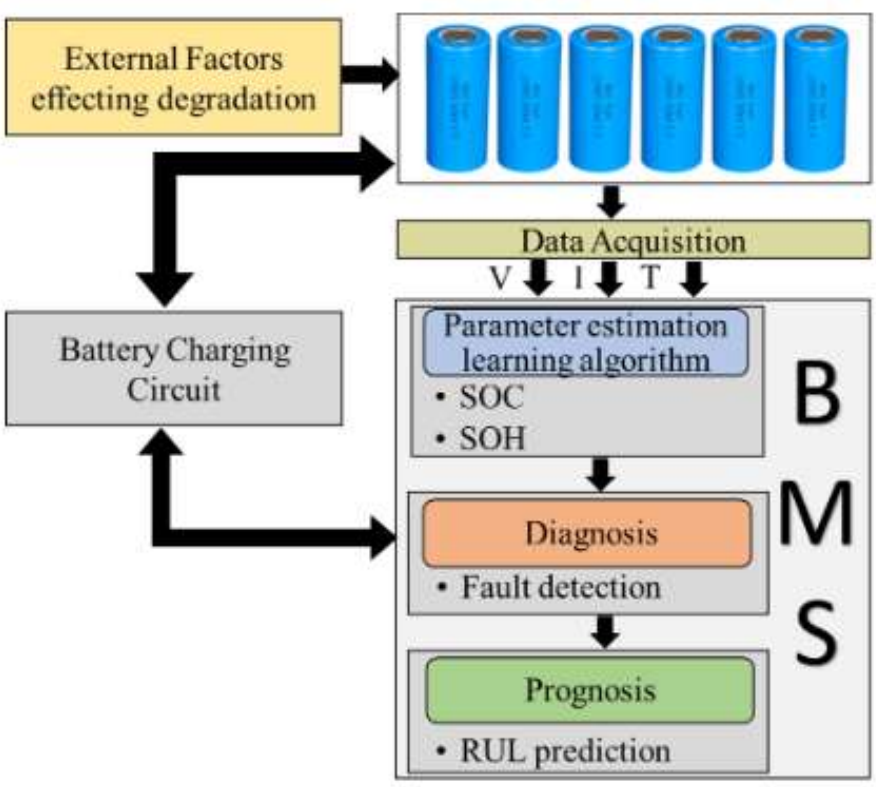

Figure 1. The architecture BMS with SOC and SOH estimation, fault diagnosis and prognosis.

The existing BMSs use linear or nonlinear dynamic models of the LIBs to estimate the SOC. Three widely used models of Li-ion battery are the electrochemical model (EChemM) *(8- 10),* electric circuit model (ECM) *(11-15),* and data-driven model *(16-21).* The ECM is widely used because of its computational efficiency compared to the EChemM and the data-driven model. The model parameters are obtained experimentally or using adaptive estimation approaches apriori to implement the SOC estimation algorithms on the BMS hardware. However, the battery model parameters vary nonlinearly with the SOC and state-of-heath (SOH) in practice. The constant parameter models for estimation may lead to an inaccurate value of SOC, leading to false range indication, which may exacerbate the "range anxiety" of the drivers. Further, the charge holding capacity of the battery is governed by the current health of the battery. Although a health-dependent parameter-varying model will improve SOC and SOH estimation, implementation of this model is challenging because the existing estimation algorithms cannot be trivially extended to time-varying dynamics. This calls for a smart BMS, i.e., BMS incorporated with self-learning and autonomous decision-making capability.

Motivated by the limitation of existing battery models and learning schemes, thus project focuses on the development of SOH-coupled varying parameter models of LIBs and self-learning algorithms to improve the autonomy and accuracy in estimation and decision-making capability of BMS. The project investigates approaches to developing SOH-coupled parameter-varying models of LIBs, which account for normal and accelerated degradation conditions, and self-learning algorithms to learn the model dynamics. The rationale behind this research is that the development of enhanced SOC and SOH coupled models and learning schemes will estimate the inter-dependent SOC and SOH simultaneously and more accurately. Taking the current health into account, this estimation approach for SOC will lead to accurate range information. Moreover, the current SOH information will precisely predict the remaining useful life of the battery based on the operational condition and usage. Nonetheless, predicting the battery's accurate range and life cycle will help transportation planners, EV manufacturers, and users design future transportation needs. Therefore, the project aligns with Tran-SET vision to use innovative techniques to overcome transportation challenges in the South-Central region.

2. OBJECTIVES

The overall objective of the proposed research project is to develop enhanced SOC and SOH dependent parameter-varying models of LIB, which account for both normal and accelerated degradation conditions, self-learning algorithms to learn the model dynamics, and fault/stress detection schemes. The overall objective of the project is divided into the following four tasks:

Task 1. The literature survey investigates various internal and external stress-inducing factors on LIBs onboard EVs and studies their effects on the capacity fade, power fade, and internal parameter variation.

Task 2. Develop an enhanced SOC and SOH-dependent parameter varying model of LIBs by accounting for normal and accelerated aging in extreme conditions.

Task 3. Develop self-learning algorithms using neural networks to learn the SOC and SOH-dependent battery model with real-time measurements.

Task 4. Develop faults/stress detection schemes using the developed model and experimentally validate the designs in the laboratory.

3. LITERATURE REVIEW

Li-ion batteries provide a cost-effective solution for high-power applications in EVs by operating the batteries at the upper-performance limits *(22)*. However, less tolerance to abuse (overcharging and discharging) and operating at the upper limits make the battery vulnerable to thermal runway leading to an explosion *(23).* This mandates a BMS for safe operation, health monitoring, and life-cycle management *(24, 25)* of the battery packs. SOC and SOH are the two key indicators, which govern battery usability and longevity, respectively. However, the highly nonlinear electrochemical dynamics and lack of embedded sensing technology to track internal parameter changes preclude the direct measurement of SOC and SOH *(26)*. Diligent efforts by multiple researchers have been put forward to estimate the SOC *(27)* and SOH *(28, 29)* in the past decade. The complexity of SOH estimation has received mainstream focus, in recent times, due to the involved challenges, including SOH dependence on several degradations accelerating factors, such as temperature, C-rate, faults, and their combinations. Moreover, the SOH and SOC also affect the internal parameters making them time-varying with degradation of health. This calls for the need for a SOH-dependent parametric model, which can be used to estimate the SOH and SOC simultaneously, and accurately for health-conscious orchestration of battery management functions.

3.1 SOH-coupled Li-ion Battery Modeling

The SOH of the battery represents the ability to store and deliver energy, which can reflect the degree of degradation. The most commonly used SOH indicators include variation in battery capacity *(30)*, DC resistance *(30)*, and AC impedance *(31)*. The development of physics-based electrochemical models *(32)* for the internal degradation mechanisms of a LIB is complex. In addition, these electrochemical models are computationally intensive to implement on low-cost target microcontrollers *(27)*. Therefore, empirical models for degradation (capacity fade) using experimental data are proposed *(33)* to reflect the cycle life aging of lithium batteries. On the other hand, as monitoring the internal temperature is one of the critical requirements for a LIB, an electro-thermal model is proposed by Lin et al. *(34)* to include the thermal effects on the battery's parameters. Later, Perez et al. *(35)* integrated the empirical aging dynamics in *(33)* (which is a function of C-rate and temperature) and electro-thermal model, in *(34)*, of the LiFePO4/graphite battery and proposed an electro-thermal-aging model. This model is established to develop optimal fast charging protocols with constant ECM parameters. The electro-thermal-aging model proposed by Perez et al. in *(35)* is extended by Pang et al. *(36)* to incorporate temperature variation in aging dynamics and ECM parameters for estimating the core and surface temperature. However, the aging dynamics used in *(35, 36)* to develop the electro-thermal-aging models did not include the dependence on one of the main aging factors, i.e., the SOC of the battery. The repeated charge-discharge at different SOC levels (depth of discharge) significantly affects the capacity fade. This dependence of capacity fade on SOC is addressed by Suri et al. *(37)*, later adapted by Liu et al. *(38)* to improve the electro-thermal-aging model. The authors in *(38)* integrated the models in *(34)* and *(35)* to compute optimal charging patterns, which accounts for the ECM parameters variation with SOC and temperature.

Besides, it has also been demonstrated by Hashemi et al. *(39)* that cell aging impacts the ECM parameters. Although all the above models in *(35, 36, 38)* integrate ECM, thermal, and capacity fade dynamics to develop an electro-thermal-aging model, the ECM employed is not coupled with the capacity fade dynamics. Thus, the effects of capacity fade (SOH) on SOC and, in turn, the

ECM parameters and the terminal voltage are not reflected, leading to inaccurate SOC and number of cycles information. Moreover, as discussed earlier, electro-thermal-aging model parameters are time-varying and nonlinear. Estimation of these time-varying ECM parameters is vital to track internal degradation, fault detection, and isolation. This requires a model that can be employed to simultaneously estimate the states (SOC and SOH) and parameters of the LIB.

3.2 Self-learning Algorithms

An ample amount of research results are available in the literature on SOC *(11, 40-46)* and 2) SOH estimation *(25)*. Kalman filters and their variants *(52-57)*, linear and nonlinear observers *(41, 58-64)*, and neural network-based offline data-driven approaches *(44, 45, 66-70)* are some of the important ones. Two common limitations of these approaches are 1) constant parameter models employed for estimation and 2) the complete apriori knowledge of model parameters, which can only be found experimentally *(71)* or estimated earlier adaptively *(42, 72-75)*. However, the model parameters vary nonlinearly with SOC *(15)*. Further, the SOC and SOH, i.e., the capacity and power fade, are interdependent and complicate the parameter dynamics. The degradation process of the battery is also accelerated due to abusive behavior *(76)*, high electro-mechanical and chemical stresses, internal faults (77-84), leading to an accelerated change in the model parameters.

It is well known that observer design and parameter estimation of time-varying dynamical systems is challenging when compared to constant parameter systems. The existing estimation algorithms cannot be trivially extended for a parameter-varying system. Developing online machine-learning algorithms that can estimate the SOC and SOH by learning the parameter-varying system from real-time measured input-output data is critical for BMS autonomy.

3.3 Fault and Stress Detection

On the other hand, the BMS is also equipped with algorithms to detect external faults, such as voltage drift, overcharge current, and high temperature *(85)*. However, the BMS cannot detect internal faults due to a lack of sensing technology *(85)*. The placement of sensors to measure the internal changes in a Li-ion battery may be difficult due to its small size and cost. An internal fault in the Li-ion battery develops high internal pressure and temperature leading to thermal runaway following ignition and explosion. Early detection and diagnosis of these faults are necessary to avoid catastrophic failures of Li-ion batteries.

Primary fault detection schemes available in the literature include co-relation-based *(87)*, model-based *(88)*, data-driven *(89)* approaches. In a correlation-based approach, the correlation coefficients of cell voltages are captured and compared for fault detection in a Li-ion battery. The limitations of the threshold-based method are the inability to differentiate faults from abrupt inputs and failure to detect faults of smaller magnitude in normal operating conditions *(90)*. Therefore, model-based fault diagnosis techniques are widely used. Model-based fault detection schemes *(91-97)* uses output error as a residual to detect a fault in the system. A fault is said to occur when this residual exceeds the threshold value. Several model-based approaches for fault detection, such as sensor faults using extended Kalman filter (EKF) *(91)*, electrochemical faults using EKF *(92)*, and sliding mode observer (SMO) *(93)*, and parameter-based faults using unscented Kalman filter (KF) *(93)*. The partial differential equation (PDE) based electrochemical model to detect internal faults was also proposed *(95)*. Simultaneous fault isolation and estimation scheme using Leuenberger and learning observers, respectively, are presented by Chen et al. *(96)*.

It is important to note that the performance of the model-based approach depends on the model accuracy with which they maintain robustness against cell-inconsistencies in all operating conditions. Although the fault detection schemes *(97-103)* mentioned above could detect and isolate various kinds of faults in Li-ion batteries, the assumptions, such as constant model parameters, linear OCV vs. SOC curve, limit their performance significantly. These assumptions are stringent in practice.

In summary, the project deals with designing algorithms for smart BMS by developing nonlinear SOC and SOH-dependent parameter varying models and associated real-time self-learning algorithms. The enhanced model and the self-learning algorithms will improve the accuracy by simultaneously estimating SOC and SOH parameters and can be employed for internal fault/stress detection.

4. METHODOLOGY

In this project, we investigated the development of SOH integrated models for LIB cells and learning algorithms to learn the model online, which was further used to estimate the SOC and SOH and detect fault/stress. We researched four steps, as mentioned under the Objective section. First, we performed a thorough literature review (Subsection 4.1) to understand the effect of degradation mechanisms on the health of the LIB. We proposed three analytical SOH-coupled models of the Li-ion cell (Subsection 4.2) based on our survey result and validated the models using both numerical and experimental data. Moreover, we proposed a real-time learning algorithm using neural networks (NN) to learn the SOH model (Section 4.3). In the final step, the SOH model with an extended Kalman filter (EKF) is employed to detect thermal fault/stress on the cell (Subsection 4.4). The details of the methodology used to develop the models and algorithms are presented in the following few subsections.,

4.1 Literature Review of Internal and External Degradation Factors (Task 1)

Motivated by the lack of a comprehensive review of LIB's health degradation and its correlation with the SOH metrics, we presented an in-depth review of the internal degradation mechanisms along with their mathematical models. We also reviewed the advanced/emerging SOH estimation methods considering both the internal and external aging effects to identify the trend and research gap that hinders intelligent BMS' development with health-conscious decision-making capability. To our best of knowledge, this is the first time such a review encompassing internal degradation and health estimation is presented in the literature.

The review focused on the following three aspects of the life cycle of the Li-ion battery:

- Internal degradation mechanisms and their modeling,
- External factors affecting the degradation of the battery, and
- Advancement in SOH estimation methods encompassing the internal degradations.

We have reviewed 179 recent journal articles and conference papers in the above categories, compiled the results in tabular forms for quick reference, and provided discussion and possible future directions for research. In addition, we systematically presented the evolution of chemical and mechanical degradation due to solid-electrolyte interface (SEI) layer formation, fracture, lithium plating, and dendrite formation and their mathematical modeling. The inter-relations among these degradation mechanisms and their effects on capacity and power fade are also discussed. The key contributions of the review are:

- We presented modeling studies on internal degradation mechanisms at anode and cathode and their relation to SOH metrics.
- The different electrochemical models, integrated with the internal degradation mechanisms and their governing equations for graphite and metal anodes commercially available, are discussed and summarized.
- The individual and combined contributions of external aging factors to capacity and power fade are discussed. The dominant degradation mechanisms under cycling and stored conditions are also reviewed.
- The empirical models of capacity and power fade for calendar and cycle aging of LIBs with different cathode chemistry are summarized in a table for quick reference. These

models can be integrated with the ECM and electrochemical models to develop SOH-integrated models.

- We reviewed the advanced SOH estimation methods accounting for the influence of both internal and external aging factors. The advantages and limitations of these advanced SOH estimation methods are summarized in a table for quick reference. In addition, the recent machine learning-based approaches and their potential to develop intelligent BMS are also presented.
- A complete section on discussion and potential future areas of research are proposed.

4.2 Development of a SOH-Coupled Parameter Varying Model of LIB

In this subsection, the development of the SOH-coupled parameter varying model of LIB is presented. This task is conducted in three steps: 1) an analytical model of the LIB is proposed by coupling the SOH and SOC dynamics and represented using a state-space formulation. 2) The model is validated numerically via simulation using MATLAB software, and 3) experimentally validated using a MACCOR battery tester. The proposed SOH-coupled analytical model is presented next.

4.2.1 Development of Analytical Model

An electro-thermal-aging model of LIB integrates a 2-RC equivalent circuit model (ECM), a thermal model, and a semi-empirical aging model.

Equivalent Circuit Model: The 2RC ECM is a combination of Thevenin and run-time circuits, as shown in Figure 2.

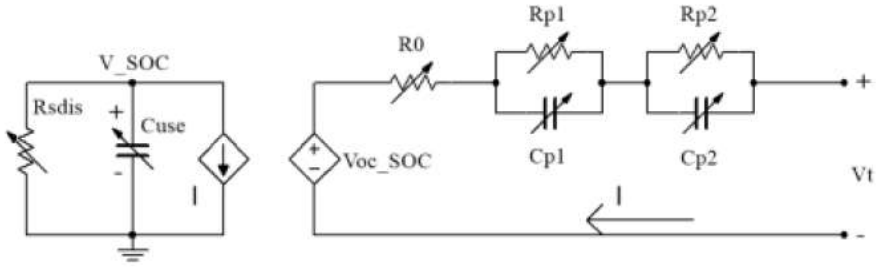

Figure 2. The two RC (2RC) equivalent circuit model (ECM) of LIB.

The ECM parameters, i.e., the circuit components $R_0, R_{p1}, C_{p1}, R_{p2}$, and C_{p2} vary with the SOC and operating temperature of the battery.

The model of ECM with the varying parameters, adapted from in *(100),* is given by

$$\frac{dSOC}{dt} = \frac{-I}{C_{use}}$$

$$\frac{dV_{c_{p1}}}{dt} = \frac{-V_{c_{p1}}}{R_{p1}(SOC,T_m)C_{p1}(SOC,T_m)} + \frac{I}{C_{p1}(SOC,T_m)}$$

$$\frac{dV_{c_{p2}}}{dt} = \frac{-V_{c_{p2}}}{R_{p2}(SOC,T_m)C_{p2}(SOC,T_m)} + \frac{I}{C_{p2}(SOC,T_m)}$$
$$V_t = V_{OC}(SOC) - V_{c_{p1}} - V_{c_{p2}} - R_0(T_m)I \quad (1)$$

where R_0 is total ohmic resistance of the cell, R_{p1} and C_{p1} are charge transfer resistance and capacitance, R_{p2} and C_{p2} are Warburg impedance and capacitance, respectively. The capacity C_{use} represents the battery's usable capacity and V_{oc} represents open-circuit voltage. The temperature T_m is the average of surface (T_s) and core (T_c) temperature given as $T_m = \frac{T_c + T_s}{2}$.

Assumption 1: The self-discharge resistance R_{sdis} has a negligible effect on the transient behavior of the battery for modeling and is neglected while modeling.

The ECM parameters dependent on SOC and T_m, adopted from *(100)*, expressed by the following equations:

$$R_{0_i} = a_{0_i} e^{\frac{a_{1_i}}{T_m - a_{2_i}}}$$
$$R_{p1_i} = (a_{3_i} + a_{4_i} SOC + a_{5_i} SOC^2) e^{\frac{a_{6_i}}{T_m - a_{7_i}}}$$
$$C_{p1_i} = a_{8_i} + a_{9_i} SOC + a_{10_i} SOC^2 + (a_{11_i} + a_{12_i} SOC + a_{13_i} SOC^2) T_m \quad (2)$$
$$R_{p2_i} = (a_{14_i} + a_{15_i} SOC + a_{16_i} SOC^2) e^{\frac{a_{17_i}}{T_m}}$$
$$C_{p2_i} = a_{18_i} + a_{19_i} SOC + a_{20_i} SOC^2 + (a_{21_i} + a_{22_i} SOC + a_{23_i} SOC^2) T_m$$

where the coefficients $a_{\tau_i} (\tau = 0,1,...,23)$ are listed in Tables 1 and 2, and the index $i \in \{c, d\}$ denotes the charging and discharging cycle of LIB.

Thermal Model: The thermal model depicts the dynamics of the core (T_c) and surface (T_s) temperatures, which are given by *(100)*,

$$\frac{dT_c}{dt} = \frac{T_s - T_c}{R_c C_c} + \frac{Q(t)}{C_c} \quad (3)$$

$$\frac{dT_s}{dt} = \frac{T_a - T_s}{R_u C_s} - \frac{T_s - T_c}{R_c C_s} \quad (4)$$

where $Q(t) = \left| I\left(V_{oc}(SOC) - V_t - T_c(t)(dV_{oc}/dT_c)\right) \right|$ is the internal heat generation, including joule heating and energy dissipated from electrodes *(102)*, and dV_{oc}/dT_c is the entropic coefficient. The heat generated from the entropic heat is neglected ($dV_{oc}/dT_c = 0$). $R_c(K/W), R_u(K/W), C_c(J/K)$ and $C_s(J/K)$ are the heat conduction resistance, convection resistance, core heat capacitance, and surface heat capacity, respectively. T_a is the ambient temperature, which is assumed to be constant.

Capacity Fade Model: The aging model, adapted from *(103)*, is given by

$$C_{loss} = (\alpha SOC + \beta) e^{\frac{E_a + \eta C_{rate}}{R_g T_c}} (Ah)^z \tag{5}$$

where C_{loss} is a function of the SOC, C_{rate} and T_c, and $C_{loss} = 20\%$ is the percentage of capacity loss in %, which is often indicative of the end of life (EOL) for an automotive battery. α, β are severity factor functions whose values depend on SOC are given in Table 4 (simulation setup section), η models the C_{rate} dependence which is given as $\eta = 152.5$, R_g is the ideal gas constant, Ah is the accumulated charge throughput, $E_a = 31500\, joule/mol$ is the activation energy and the power-law factor $z = 0.57$. Based on Eq. (5) the SOH can be defined as,

$$SOH(t) = SOH(t_0) - \frac{\int_{t_0}^{t} |I(\tau)|\, d\tau}{2N(SOC, C_{rate}, T_c) C_{use}} \tag{6}$$

where t_0 denotes the initial time. Consequently, $SOH = 1$ for a new battery and $SOH = 0$ corresponds to 20% capacity loss. The time derivative of Eq. (6) yields the battery aging model given by

$$\frac{dSOH}{dt} = -\frac{|I(t)|}{2N(SOC, C_{rate}, T_c) C_{use}} \tag{7}$$

where N denotes the number of cycles until EOL, which is given as

$$N(SOC, C_{rate}, T_c) = \frac{3600 Ah_{total}(SOC, C_{rate}, T_c)}{C_{use}} \tag{8}$$

where Ah_{total} is the total amount of charge that can flow in and out of the battery during its operation and expressed by

$$Ah_{total} = \left[\frac{20}{(\alpha SOC + \beta) e^{\frac{-E_a + \eta C_{rate}}{R_g T_c}}} \right]^{\frac{1}{z}} \tag{9}$$

Remark 1: The dynamics in Eq. (1), (3), (4), and (7) can be combined to form an electro-thermal -aging model. However, straightforward integration of these models will not reflect the interdependency of the capacity fade in Eq. (7) on SOC dynamics in Eq. (1) (first equation) and, therefore, the effects on parameter variation. Furthermore, since the usable capacity keeps diminishing from the design/nominal capacity as the battery ages *(101)*, the usable capacity in the SOC dynamics Eq. (1) must be coupled with the SOH dynamics in Eq. (7).

Model-integration and Proposed SOH-coupled Model: To couple the Eq. (7) to the dynamics of SOC in Eq. (1) (first equation), we redefined the SOC dynamics as

$$\frac{dSOC}{dt} = \frac{-I(t)}{SOH(t)C_{use}}. \tag{10}$$

For completeness, the proposed SOH-coupled electro-thermal-aging model by incorporating the coupling term in Eq. (10) can be expressed as

$$\begin{aligned}
\frac{dSOC}{dt} &= \frac{-I}{SOHC_{use}} \\
\frac{dV_{c_{p1}}}{dt} &= \frac{-V_{c_{p1}}}{R_{p1}(SOC,T_m)C_{p1}(SOC,T_m)} + \frac{I}{C_{p1}(SOC,T_m)} \\
\frac{dV_{c_{p2}}}{dt} &= \frac{-V_{c_{p2}}}{R_{p2}(SOC,T_m)C_{p2}(SOC,T_m)} + \frac{I}{C_{p2}(SOC,T_m)} \\
\frac{dT_c}{dt} &= \frac{T_s - T_c}{R_cC_c} + \frac{I(V_{c_{p1}} + V_{c_{p2}} + R_0(T_m)I)}{C_c} \\
\frac{dT_s}{dt} &= \frac{T_a - T_s}{R_uC_s} - \frac{T_s - T_c}{R_cC_s} \\
\frac{dSOH}{dt} &= -\frac{|I(t)|}{2N(SOC,C_{rate},T_c)C_{use}}.
\end{aligned} \tag{11}$$

Note that the term $Q(t)$ is eliminated using the terminal voltage equation of the battery. The modeling process and the steps involved in formulating the model are shown in Figure 3.

Now, define the states of the system as $x = [x_1 \;\; x_2 \;\; x_3 \;\; x_4 \;\; x_5 \;\; x_6]^T \in \mathbb{R}^6$ with $x_1 = SOC$, $x_2 = V_{c_{p1}}$, $x_3 = V_{c_{p2}}$, $x_4 = T_c, x_5 = T_s,$ and $x_6 = SOH$ with $T_m = \frac{x_4 + x_5}{2}$ and the control input $u \in \mathbb{R}$. The state-space model of the SOH-coupled electro-thermal-aging dynamics are given in a non-affine form as follows,

$$\begin{aligned}
\dot{x} &= f^s(x,u) \\
y &= h^s(x,u)
\end{aligned} \tag{12}$$

where the output equation $h^s(x,u) = V_{OC}(x_1) - x_2 - x_3 - R_0(x_4,x_5)u$ and the internal dynamics denoted by

$$\begin{aligned}
f^s(x,u) = \Bigg[& \frac{-u}{x_6C_{use}}, \frac{-x_2}{R_{p1}(x_1,x_4,x_5)C_{p1}(x_1,x_4,x_5)} + \frac{u}{C_{p1}(x_1,x_4,x_5)}, \frac{-x_3}{R_{p2}(x_1,x_4,x_5)C_{p2}(x_1,x_4,x_5)} \\
& + \frac{u}{C_{p2}(x_1,x_4,x_5)}, \frac{-x_4}{R_cC_c} + \frac{x_5}{R_cC_c} + \frac{u(x_2 + x_3 + R_0(x_4,x_5)u)}{C_c}, \frac{x_4}{R_cC_s} - \frac{x_5}{R_uC_s} - \frac{x_5}{R_cC_s} + \frac{T_a}{R_uC_s}, \frac{-u}{2N(C_{rate},x_1,x_4)C_{use}} \Bigg]^T.
\end{aligned}$$

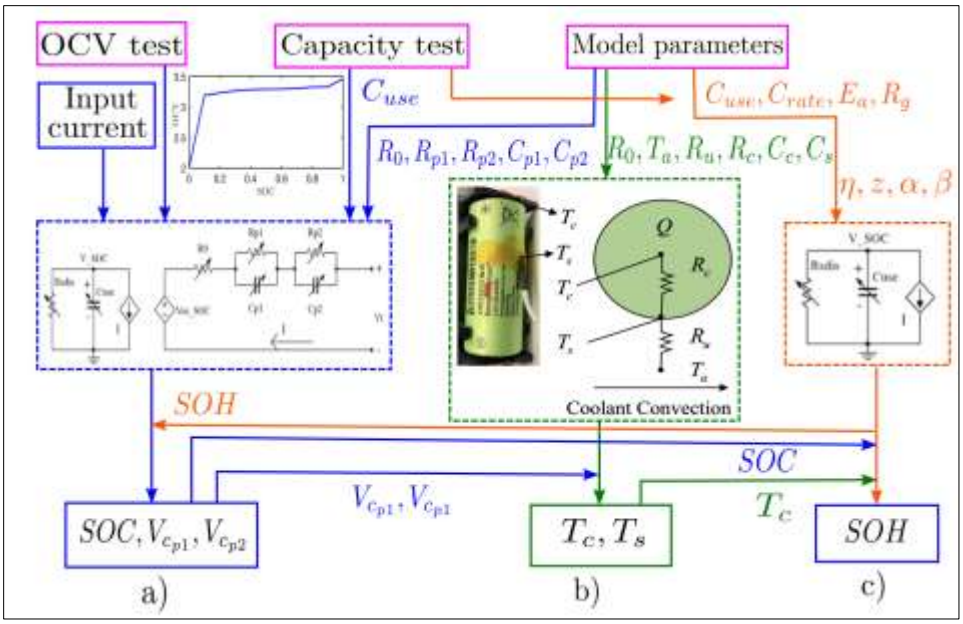

Figure 3. SOH-coupled model of LIB a) ECM, b) thermal model, c) capacity fade model.

4.2.2 Kalman Filter for State Estimation

The goal is to simultaneously estimate the SOC, SOH T_c, and T_s for the model developed in Eq. (12) using an EKF. For the ease of onboard implementation, the discrete-time representation of the SOH-coupled thermal model can be expressed as

$$\begin{aligned} x_{k+1} &= f^s(x_k, u_k) \\ y_k &= h^s(x_k, u_k) + v_k \end{aligned} \tag{13}$$

We have used Euler's approximation to discretize the model. The nonlinear function $f^s(x_k, u_k)$ is the discrete internal dynamic function and $h^s(x_k, u_k)$ is the output function. An observation noise v_k is included to account for the measurement noise. The estimated state is denoted by $\hat{x}_k$, $u_k \in \mathbb{R}$ and $y_k \in \mathbb{R}$ are the control input and output, respectively, at time instant $k \in \mathbb{N}$, $\mathbb{N} = 1, 2, 3\cdots$ with a sampling period T, i.e., $t = kT$.

The process of EKF uses two steps: update and prediction, as shown in Algorithm 1. The prediction step is used to estimate the state and covariance matrix $P_{k|k-1} \in \mathbb{R}^{n\times n}$. The update step is used to update the state and covariance estimates using the Kalman gain $K_k \in \mathbb{R}^n$, residual covariance matrix $S_k \in \mathbb{R}^{m\times m}$, measurement variance matrix $R_k \in \mathbb{R}^{m\times m}$, and measurement matrix H_k. The state transition and observation matrices F_k^H and H_k, respectively, are given as,

$$\begin{aligned} F_k^H &= \frac{\partial f^H}{\partial x}\Big|_{\hat{x}_{k-1|k-1}, u_k} \\ H_k &= \frac{\partial h}{\partial x}\Big|_{\hat{x}_{k|k-1}, u_k}. \end{aligned} \tag{14}$$

Table 1. Algorithm for the extended Kalman filter

Algorithm 1: Extended Kalman filter		
Step 1:	Initialize $k= 0$ Initialize state vector and covariance matrix $\hat{x}_0^- = E(x_0), P_0^- = E[(x_0 - \hat{x}_0^-)(x_0 - \hat{x}_0^-)^T]$	
Step 2:	Computation $k = 1, 2, ...$ Prediction Step: $\hat{x}_{k\|k-1} = f(\hat{x}_{k-1\|k-1}) + g(\hat{x}_{k-1\|k-1})u_k$	→ Predicted state estimate
	$\hat{y}_k = h(\hat{x}_{k\|k-1}, u_k)$	
	$P_{k\|k-1} = F_k P_{k-1\|k-1} F_k^T + Q_k$	→ Predicted covariance estimate
Step 3:	Update Step: $\tilde{y}_k = y_k - \hat{y}_k$	→ Error
	$S_k = H_k P_{k\|k-1} H_k^T + R_k$	→ Residual covariance
	$K_k = P_{k\|k-1} H_k^T S_k^{-1}$	→ Optimal Kalman gain
	$\hat{x}_{k\|k} = \hat{x}_{k\|k-1} + K_k \tilde{y}_k$	→ Updated state estimation}
	$P_{k\|k} = (I - K_k H_k) P_{k\|k-1}$	→ Updated covariance estimation}

4.2.3 Model Validation

We have validated the proposed model both experimentally and numerically. The MACCOR battery tester and MATLAB software are used for the validation. We also employed the EKF to estimate the internal states of the battery using the measured voltage output. A detailed discussion on the model validation is presented below.

Simulation Setup: The widely used cylindrical A123 26650 LiFePO4/graphite cell was chosen for the simulation study. The parameters used for simulation are as follows:

The coefficients of the model parameters in Eq. (2) for charging and discharging, obtained from the experimental data presented in *(100)*, are given in Table 2 and Table 3.

Table 2. Coefficients (charge).

$a0_c$ =0.0055	$a8_c$=0.0113	$a16_c$= -131.2298
$a1_c$ = 22.2477	$a9_c$= -0.027	$a17_c$=162.4688
$a2_c$=-11.5943	$a10_c$= 0.0339	$a18_c$ = 6.2449E4
$a3_c$ =0.0016	$a11_c$=17.0224	$a19_c$=-1.055E5
$a4_c$= -0.0032	$a12_c$=523.215	$a20_c$=4.4432E4
$a5_c$ = 0.0045	$a13_c$= 6.4171E3	$a21_c$=198.9753
$a6_c$= 159.2819	$a14_c$= -7.5555E3	$a22_c$=7.5621E3
$a7_c$=-41.4548	$a15_c$=50.707	$a23_c$= -6.9365E3

Table 3. Coefficients (discharge)

a_{0_c} =0.0048	a_{8_c}=0.0288	a_{16_c}= -65.4786
a_{1_c} = 31.0494	a_{9_c}= -0.073	a_{17_c}=44.3761
a_{2_c}=-15.3253	a_{10_c}= 0.0605	a_{18_c} = 3.1887E4
a_{3_c} =7.1135E-4	a_{11_c}=16.6712	a_{19_c}=-1.1593E5
a_{4_c}= -4.3865E-4	a_{12_c}=335.4518	a_{20_c}=1.0493E4
a_{5_c} = 2.3788E-4	a_{13_c}= 3.1712E3	a_{21_c}=60.3114
a_{6_c}= 347.4707	a_{14_c}= -1.3214E3	a_{22_c}=1.0175E4
a_{7_c}=-79.5816	a_{15_c}=53.2138	a_{23_c}= -9.524E3

The parameters of a single cell lumped thermal model adapted from *(104)* were chosen as $R_u = 3.08$, $R_c = 1.94$, $C_c = 62.7$, $C_s = 4.5$, and $R_g = 8.314$ *(100)*. The SOH model parameters α, β, whose values depend on SOC, are given in Table 4, $\eta = 152.5$, R_g is the ideal gas constant, $E_a = 31500\, joule/mol$ and $z = 0.57$.

Table 4. Optimal values of α and β.

$SOC\%$	α	β
$SOC\% < 45$	2896.6	7411.2
$SOC\% \geq 45$	2694.5	6022.2

The cell's capacity is measured experimentally by cycling the battery at low C_{rate} (C/20) and found to be \$2.4 Ah\$. The $V_{oc}(SOC)$ curve is obtained from a standard OCV-SOC test as follows:

1) The batteries were fully discharged to 0% SOC following the standard constant current constant voltage (CC-CV) protocol, as shown in Figure 4.
2) The batteries were rested for 2 hours.
3) The batteries were charged with C/20 at intervals of 10% SOC.
4) The OCV of batteries was measured after 2 hours rest after each 10% SOC increment.
5) Steps 3) and 4) were repeated until the batteries were charged to 100% SOC.
6) Steps 3), 4) and 5) were repeated for discharge protocol.

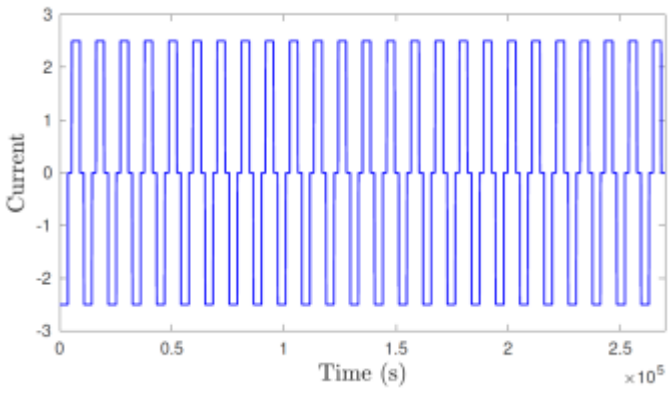

Figure 4. CC-CV current in A at 1 C-rate.

The OCV vs SOC curve obtained from the experimental result is shown in Figure 5. The average of these curves is used to model the $V_{oc}(SOC)$. It can be observed that $V_{oc}(SOC)$ has an almost linear behavior in the region between 10% and 100% SOC and exponentially drops while the SOC is approximately below 10% *(105)*. Although V_{oc} varies with temperature, it is shown in *(106)* that the variation is minimal in $LiFePO_4$ cells. So, OCV-SOC test is carried out at $25^{\circ}C$.

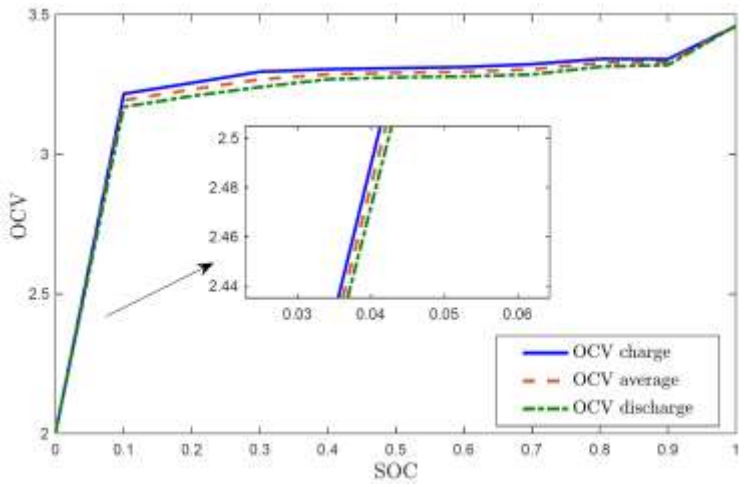

Figure 5. OCV vs SOC curve obtained from the experiment.

The expression for the V_{oc} by fitting the curve is obtained as

$$V_{oc}(SOC) = p_0 + p_1 SOC + p_2 SOC^2 + p_3 SOC^3 + p_4 SOC^4 + p_5 SOC^5 + p_6 SOC^6 + p_7 SOC^7 \quad (15)$$

where the coefficients $p_{(.)}$ are given the Table 5.

Table 5. Coefficients $p_{(.)}$ of the V_{OC} expression.

p_0 =2.008	p_3= 854.1	p_6=-1539
p_1 = 25.87	p_4=-1911	p_7= 404.9
p_2 = -209.4	p_5=2376	

The initial state vector is selected as $x = [0, 0.1, 0.1, 10, 25, 1]^T$ with a sampling time of 1s. Then, a 10A (approx. 4.17 C-rate) CC-CV charge-discharge cycle is used as an input to observe the battery degradation over the life at $T_a = 25^0 C$. The finding of the numerical experiment is discussed in detail in Section 5.

Experimental Setup: We validated the models using A123 26650 LiFePO4/graphite cells with a capacity of 2.5 Ah. The battery test bench, shown in Figure 6 and Figure 7, consists of the following test equipment.

- The MACCOR 4300 M battery testing system
- Environmental chamber
- Host PC with battery cycling software

The testing system records the battery's measured data (voltage, current, and temperature) to the computer with the sampling time of one second. The user interface and data visualization windows are shown in Figure 8.

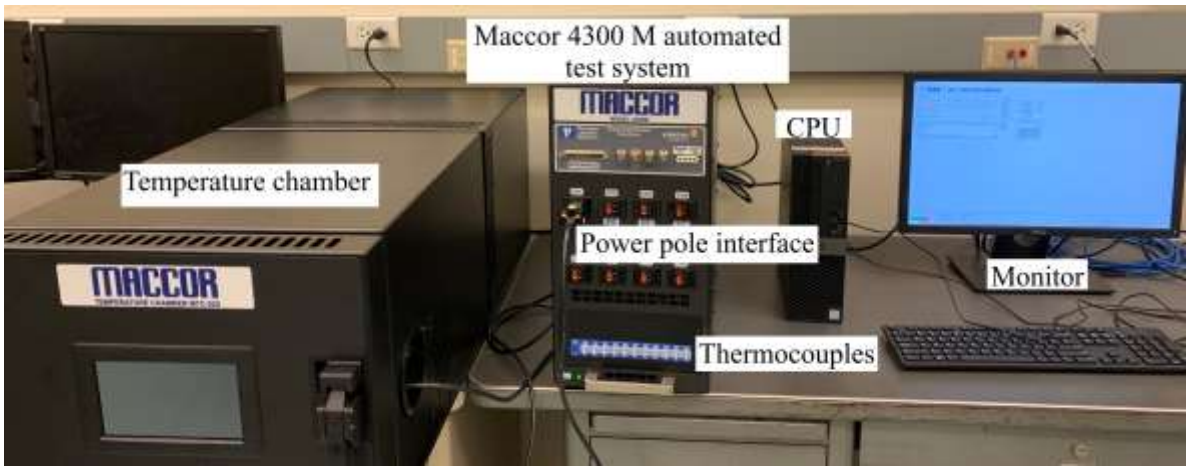

Figure 6. Battery test equipment for experimental validation.

Figure 7. A123 26650 and 18650 Li-ion batteries (a) outside the environmental chamber at room temperature and (b) inside the environmental chamber with controlled temperature.

The battery cycling software is used to program the charging and discharging current. A constant current and constant voltage (CC-CV) charge-discharge pattern at 1 C-rate is used for the experimental validation. The software is also equipped with plotting options to visualize the charge-discharge voltage, current, and power fade, as shown in Figure 10 and Figure 11.

However, the host PC does not permit the installation of other analysis software, such as MATLAB. We imported the recorded current and voltage to MATLAB to validate the proposed coupled model in Eq. (12).

The following steps are employed for the validation of the model.

1. The A123 26650 cylindrical cell is cycled at a 1C-rate inside the environmental chamber at a temperature of 25 deg. for 52 cycles.

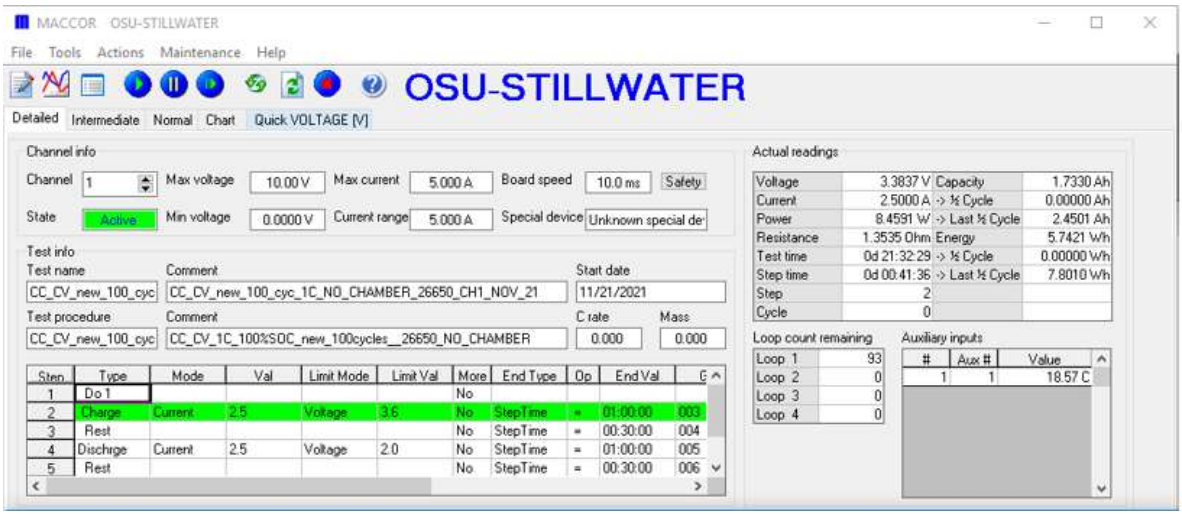

Figure 8. MACCOR user interface for battery testing.

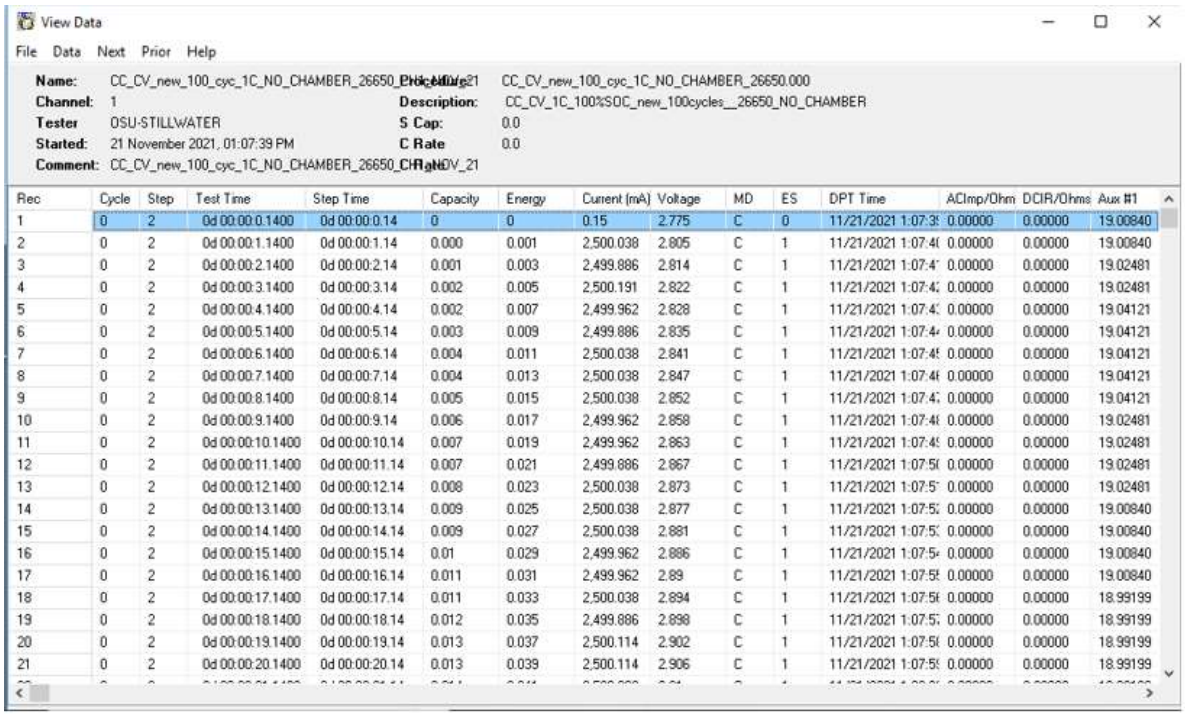

Figure 9. Data visualization using MACCOR interactive displays.

2. The voltage, current, and temperature data acquired from the battery tester are stored in the host PC in a .txt file format.
3. The data files are exported to the PC with MATLAB software.
4. The CC-CV current used to cycle the battery is used for the model developed in Eq. (12).
5. The output voltage of the simulated model and the experimentally measured voltage are compared to validate the error.

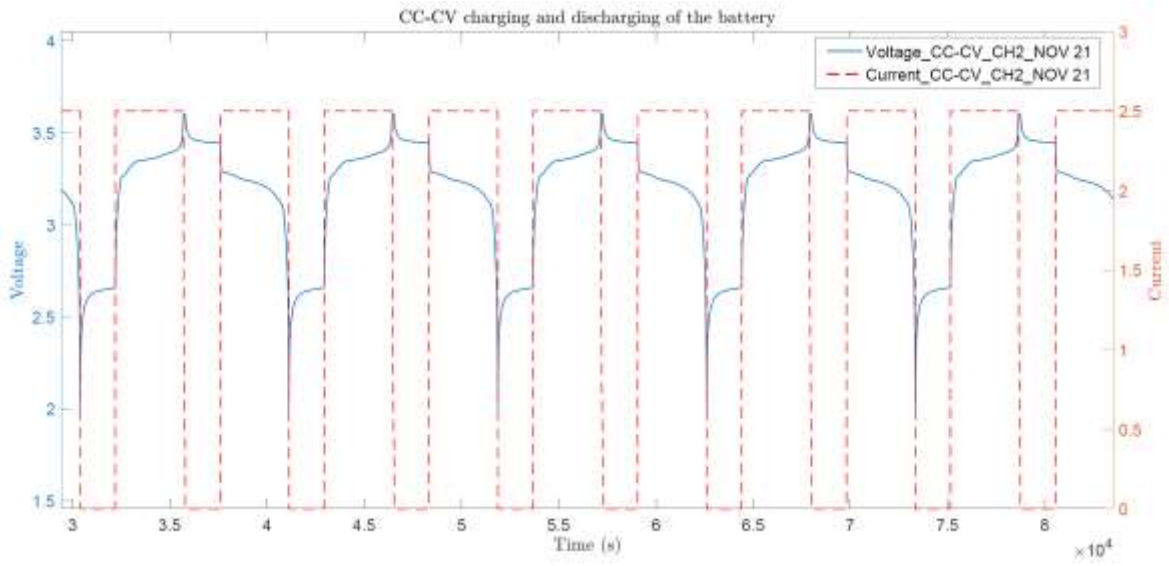

Figure 10. Constant current and constant voltage charging and discharging of the battery.

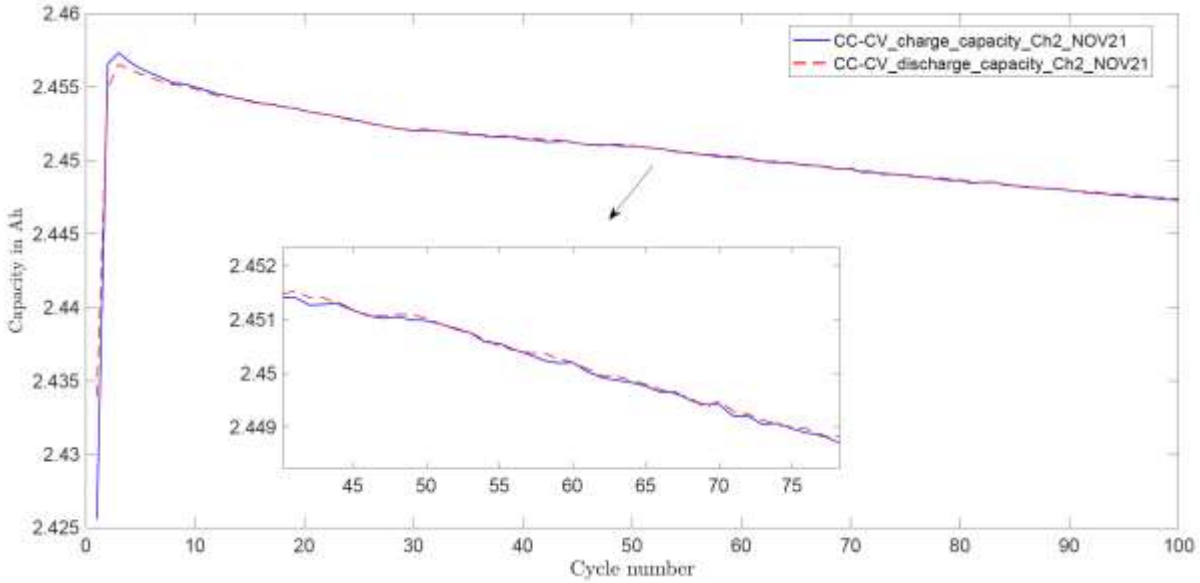

Figure 11. Capacity loss of the battery with an increased number of charge-discharge cycles.

The findings are discussed in Section 5.

4.3 Self-learning Algorithm for SOH

In this task, we focused on developing real-time machine learning algorithms using neural networks to learn the SOH-coupled model developed in Task 2. However, the proposed SOH coupled model in Eq. (12) has two nonlinearities: the nonlinear state and output equations. To learn the complete model, we need two neural networks (one for the state and one for the output), which will require more computation for implementation purposes. Therefore, we first reformulated the model to integrate the output equation in the state dynamics. Then, we proposed real-time machine learning algorithms using neural networks (NNs), which can learn the model

using measured voltage, current, and temperature. In the following sections, we have presented the methodologies for model reformulation and the development of an NN-based identifier to learn the system model.

4.3.1 Model Reformulation for Self-learning Algorithm

The state-space model in Eq. (12) is reformulated by redefining the states vector to incorporate the terminal voltage V_t. We further expressed the voltage V_{cp2} in terms of other ECM parameters. This helped keep the number of states equal. The new states are $x_1 = SOC$, $x_2 = V_{c_{p1}}$, $x_3 = T_c, x_4 = T_s, x_5 = SOH,$ and $x_6 = V_t$. We also refined the inputs as $u = [u_1 \ u_2]^T$, where $u_1 = I$, and $u_2 = T_a$.

The voltage across the second RC pair, $V_{c_{p2}}$, defined as a state in Eq. (12), is rewritten as

$$V_{c_{p2}} = \beta(x_1) - x_6 - x_2 - R_0(x_3, x_4)u_1. \tag{16}$$

Substituting the value of $V_{c_{p2}}$ from Eq. (16) in dynamics of voltage and rearranging the terms gives

$$\begin{aligned}\dot{V}_t = {} & \alpha(x_1, x_3, x_4, x_6, u_1, u_2) + x_2\left[\frac{1}{R_{p1}(x_1, x_3, x_4)C_{p1}(x_1, x_3, x_4)} - \frac{1}{R_{p2}(x_1, x_3, x_4)C_{p2}(x_1, x_3, x_4)}\right] \\ & - x_6\left[\frac{1}{R_{p2}(x_1, x_3, x_4)C_{p2}(x_1, x_3, x_4)}\right] - u_1\left[\frac{1}{C_{p1}(x_1, x_3, x_4)} + \frac{1}{C_{p2}(x_1, x_3, x_4)}\right. \\ & \left. + \frac{R_0(x_3, x_4)}{R_{p2}(x_1, x_3, x_4)C_{p2}(x_1, x_3, x_4)}\right] + \frac{\beta(x_1)}{R_{p2}(x_1, x_3, x_4)C_{p2}(x_1, x_3, x_4)}\end{aligned} \tag{17}$$

where $\alpha(x_1, x_3, x_4, x_6, u_1, u_2) = -u_1\dot{R}_0(x_3, x_4)\left(\frac{x_4 - x_3}{2R_cC_c} + \frac{u_1(\beta(x_1) - x_6)}{2C_c} + \frac{u_2 - x_4}{2R_uC_s} - \frac{x_4 - x_3}{2R_cC_s}\right)$.

The dynamics of voltage Eq. (17), the state-space model is redefined as

$$\begin{aligned}\dot{x} &= f^{NN}(x, u) \\ y &= C^{NN}x\end{aligned} \tag{18}$$

where $C^{NN} = \begin{bmatrix} 0 & 0 & 0 & 0 & 0 & 1 \\ 0 & 0 & 0 & 1 & 0 & 0 \end{bmatrix}$ is the linear output coefficient matrix and the internal dynamics

$$f^{NN}(x, u) = \left[\frac{-u_1}{x_5C_{use}}, \frac{-x_2}{R_{p1}(x_1, x_3, x_4)C_{p1}(x_1, x_3, x_4)} + \frac{u_1}{C_{p1}(x_1, x_3, x_4)}, \frac{-x_3}{R_cC_c} + \frac{x_4}{R_cC_c} + \frac{u_1(x_6 - \beta(x_1))}{C_c}\right.$$

$$\left.\frac{x_3}{R_cC_s} - \frac{x_4}{R_uC_s} - \frac{x_4}{R_cC_s} + \frac{u_2}{R_uC_s}, \frac{-u_1}{2N(C_{rate}, x_1, x_3)C_{use}}, f_6(x, u)\right]^T,$$

where $f_6(x, u) = \dot{V}_t$ as defined in Eq. (17).

Remark 2: The model in Eq. (18) has a linear output map, and the output matrix C^{NN} is known. Therefore, we can employ one NN to learn the system model presented next.

4.3.2 Neural Network-based Identifier

In this section, we have designed the NN-based identifier. The LIB model in Eq. (18) can be rewritten as

$$\begin{aligned} \dot{x} &= Ax + \overline{f}^{NN}(x,u) \\ y &= C^{NN}x \end{aligned} \tag{19}$$

where $\overline{f}^{NN}(x,u) = f^{NN}(x,u) - Ax$ with A is a stable matrix of appropriate dimensions. By universal approximation property of the neural network, one can express a nonlinear function $g(x) \in \mathbb{R}^n$ as

$$g(x) = W^T \phi(x) + \grave{o}(x) \tag{20}$$

where $W \in \mathbb{R}^{l \times n}$ is the unknown weight vector and $\phi(x) \in \mathbb{R}^l$ is the activation function with l is the number of neurons, and $\grave{o}(x) \in \mathbb{R}^n$ is the approximation error. Two-layer neural network architecture is shown in Figure 12, is used to approximate the internal dynamics f^{NN}.

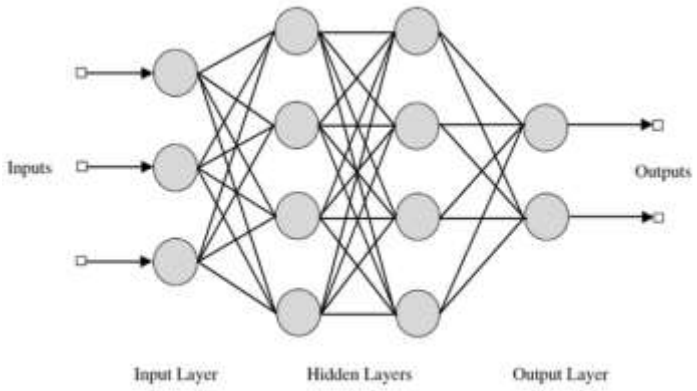

Figure 12. Two-layer neural network for learning the lithium-ion battery model.

Recalling the LIB dynamics in Eq. (19), with NN approximation in Eq. (20), the system dynamics can be approximated as

$$\dot{x} = Ax + \theta^T \sigma(x,u) + \grave{o}(x,u)$$

where $A \in \mathbb{R}^{n \times n}$ is a Hurwitz matrix, $\grave{o}(x,u)$ is the approximation error, $\theta^T \in \mathbb{R}^{n \times l}$ is unknown ideal NN weight matrix, $\sigma(x,u) \in \mathbb{R}^l$ is vector basis functions, l is the number of neurons in the neural network architecture.

Assumption 2: The NN target weight matrix, activation function, and the approximation errors are bounded and satisfy $\|\theta\| \le \theta_{\max}$, $\|\sigma(x,u)\| \le \sigma_{max}$ and $\| \grave{o}(x,u) \| \le \grave{o}_{max}$ where $\theta_{\max}$, σ_{max}, and $\grave{o}_{max}$ are unknown positive constants.

This is a standard assumption in NN literature. With the estimated NN weights, the identifier can be expressed as

$$\begin{aligned}\dot{\hat{x}} &= \hat{\theta}^T \sigma(\hat{x},u) + A\hat{x} + L^T \tilde{y} \\ \hat{y} &= C\hat{x}\end{aligned} \tag{21}$$

where $\hat{x}$ is the estimated state and $\hat{\theta} \in \mathbb{R}^{n \times l}$ is the estimated NN weight matrix to be updated to minimize the state estimation error defined by $e_x = x - \hat{x}$.

Since the state estimation error is not available for measurement, we will use the output estimation error is defined as $e_y = y - \hat{y}$, to update the NN weights. The weight update law designed using Lyapunov based approach is described next.

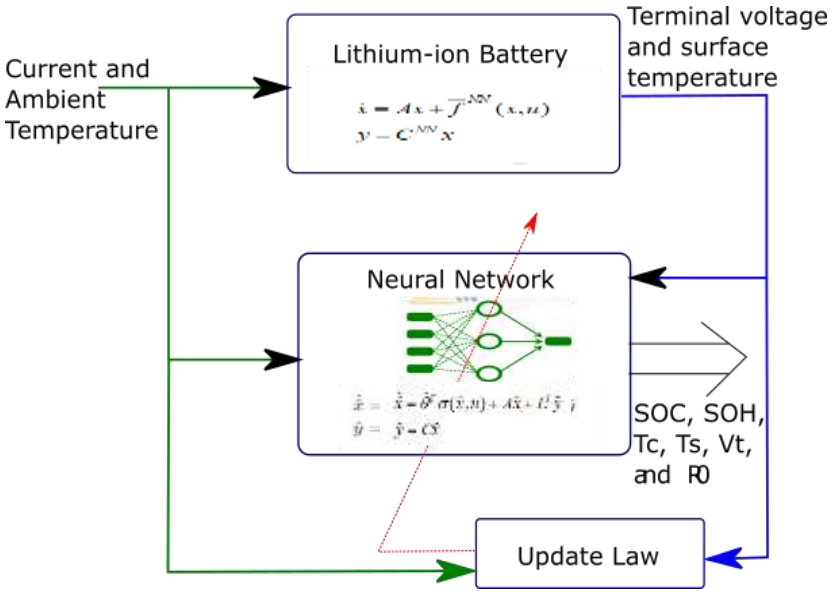

Figure 13. The architecture of the NN-based model-learning mechanism.

The goal of designing an update law for the NN weights is to minimize the state estimation error e_x. Define a recursive least square NN weight update law as

$$\dot{\hat{\theta}} = \tau P_1 \sigma(\hat{x},u) \tilde{y}^T M \tag{22}$$

$$\dot{P}_1 = -\alpha \frac{P_1 \sigma(\hat{x},u) \sigma^T(\hat{x},u) P_1}{1 + \left\| \sigma^T(\hat{x},u) \sigma(\hat{x},u) \right\|} \tag{23}$$

where M is a dimension matching matrix, α, τ are hyper-parameters for tunning and P_1 is a user-defined positive definite matrix. A block diagram of the learning mechanism is shown in Figure 13 below.

Remark 3: The NN weights are updated online with real-time measurements. The learning gains (hyper-parameters) can be chosen using the conditions derived from the Lyapunov stability analysis,

To validate the analytical design of the learning algorithm, we run a computer simulation using MATLAB with the parameters design in Section 4.4. The details of the analysis and findings are provided in Section 5.

4.4 Fault Detection Scheme

In this task, we developed a fault detection scheme using the model proposed in Section 4.2. We reformulated the model to incorporate the time-varying internal resistance as a dynamical state to estimate the battery's internal resistance using a filter-based approach. This allows us to isolate the internal faults. We then implemented an extended Kalman Filter (EKF) to estimate the states and developed a model-based fault detection algorithm to detect a thermal fault. The following section presents the methodology employed for model reformulation, EKF algorithm, and fault detection scheme in detail.

4.4.1 Model-reformulation for Fault Detection

The SOH coupled model in Eq. (12) is reformulated by including the internal resistance as the seventh state of the system. The state vector can be written as $x = [x_1 \ x_2 \ x_3 \ x_4 \ x_5 \ x_6 \ x_7]^T$ where $x_1 = SOC$, $x_2 = V_{c_{p1}}$, $x_3 = V_{c_{p1}}$, $x_4 = T_c, x_5 = T_s, x_6 = SOH, x_7 = R_0$, The new state-space model in a non-affine form is given as,

$$\begin{aligned} \dot{x} &= f^p(x,u) \\ \overline{y} &= h^p(x,u) \end{aligned} \tag{24}$$

where $h^p = V_{oc}(x_1) - x_2 - x_3 - x_7 u$ and the internal dynamics are denoted by

$$f^p(x,u) = \left[\frac{-u}{x_6 C_{use}}, \frac{-x_2}{R_{p1}(x_1,x_4,x_5)C_{p1}(x_1,x_4,x_5)} + \frac{u}{C_{p1}(x_1,T_m)}, \frac{-x_3}{R_{p2}(x_1,x_4,x_5)C_{p2}(x_1,x_4,x_5)} + \frac{u}{C_{p2}(x_1,T_m)} \right.$$

$$\left. \frac{-x_4}{R_c C_c} + \frac{x_5}{R_c C_c} + \frac{u(x_2+x_3+x_7)u)}{C_c}, \frac{x_4}{R_c C_s} - \frac{x_5}{R_u C_s} - \frac{x_5}{R_c C_s} + \frac{T_a}{R_u C_s}, \frac{-u}{2N(C_{rate},x_4)C_{use}}, f_r(x_4,x_5) \right]^T$$

with $f_r(x_4,x_5) = dR_0/dt$ computed from Eq. (2).

Remark 4: The above state-space representation uses the SOH-dependent ECM parameter R_0 as a state of the system. Therefore, the change in parameters can be estimated using observer or filter-based approaches.

4.4.2 Model-based Fault Detection using Kalman Filter

A model-based fault detection scheme is developed using the proposed discrete-time model in Eq. (13) and the EKF algorithm presented in Section 4.1.D. The model-based fault detection scheme compares the EKF output with the LIB output to generate the output residual. Since the EKF is unaware of the fault, the difference between the battery terminal voltage and EKF output increases. This error is, in general, referred to as fault detection residual. The residual is compared with the detection threshold to detect the fault. A schematic of the model-based fault detection employed

in our project is shown in Figure 14. We carried out the numerical simulation of the reformulated model, EKF, and the fault detection scheme using MATLAB.

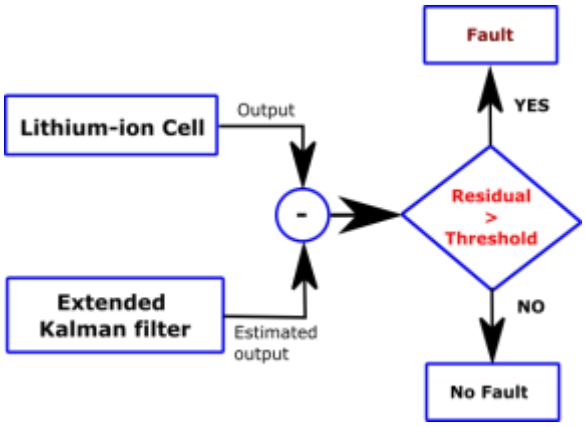

Figure 14. The architecture of the model-based fault detection system.

The following methodology was used to validate the fault detection algorithm via numerical simulation:

1. The LIB model in Eq. (24) is discretized using Euler's approach and used as the LIB block, shown in Figure 14. The parameters of the model are defined in Section 4.2.3.
2. The EKF described in Section 4.2.2 is employed as the fault detection observer or model.
3. A slowly rising exponential fault is introduced in the model only to mimic the thermal fault in the battery.
4. The residual is generated by comparing the battery model output and the EKF output.
5. The knowledge of the LIB parameters is used to determine the fault detection threshold. The details of the results are discussed in Section 5.

5. ANALYSIS AND FINDINGS

This section presents the research findings from the methodology of the tasks described in the previous section in detail.

5.1 Findings from the Literature Review (Task 1)

We have reviewed internal degradation mechanisms, shown in Figure 15, such as SEI layer formation, fracture, lithium plating, and dendrite formation in detail, along with their modeling. The studies show that the internal degradation steps from SEI formation to lithium plating can be summarized as follows:

1. SEI layer grows substantially at the anode with consecutive charge and discharge cycles.
2. Due to SEI's permeability to Li-ions, significant stresses are generated, leading to fractures of electrodes.
3. SEI layer formation and its growth reduce anode's porosity, resulting in Li-plating or Li-metal formation at the narrow gap between the anode and the electrolyte.
4. Li-plating again results in protrusions on the electrode surface, leading to dendrites.

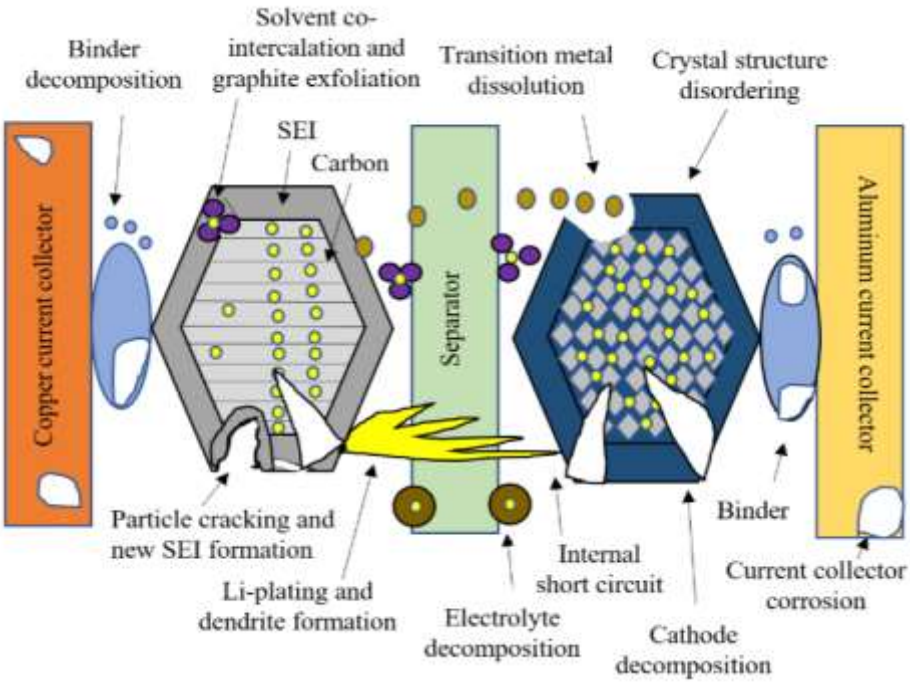

Figure 15. Internal degradation mechanisms in Li-ion cells adapted from *(98)*.

It is well established that the dominant aging mechanisms for graphite anode Lithium-ion batteries (LIBs) are SEI formation, which increases the impedance and the consumption of Li-ions. Additionally, lithium metal plating could also contribute to accelerated aging, causing a further increase in capacity and power fade. On the other hand, cathode materials in LIBs are significantly affected by both cycling and calendar life. The characteristics of the cathode may differ from one chemistry to another due to their sensitivities to aging. Thus, the degradation mechanisms can be clustered into loss of lithium-ions (LLI), loss of active material (LAM) - anode, LAM – cathode, and increase of the faradic and ohmic resistances. We further concluded that while

the fracture, lithium plating, and dendrite formation lead to loss of active lithium resulting in capacity loss, the SEI layer formation affects both the capacity loss and power fade. We have tabulated the results.

We also investigated the effects of external factors that accelerate the degradation process in the battery, such as temperature, charge/discharge rate, depth of discharge (DOD), time, voltage effects during cycling, and SOC during rest periods. A cause and effect diagram depicting the influence of the external factors on the internal degradation mechanism with their corresponding degradation modes (LLI, LAM, loss of cathode material) and effects on the capacity and power fade is shown in Figure 16.

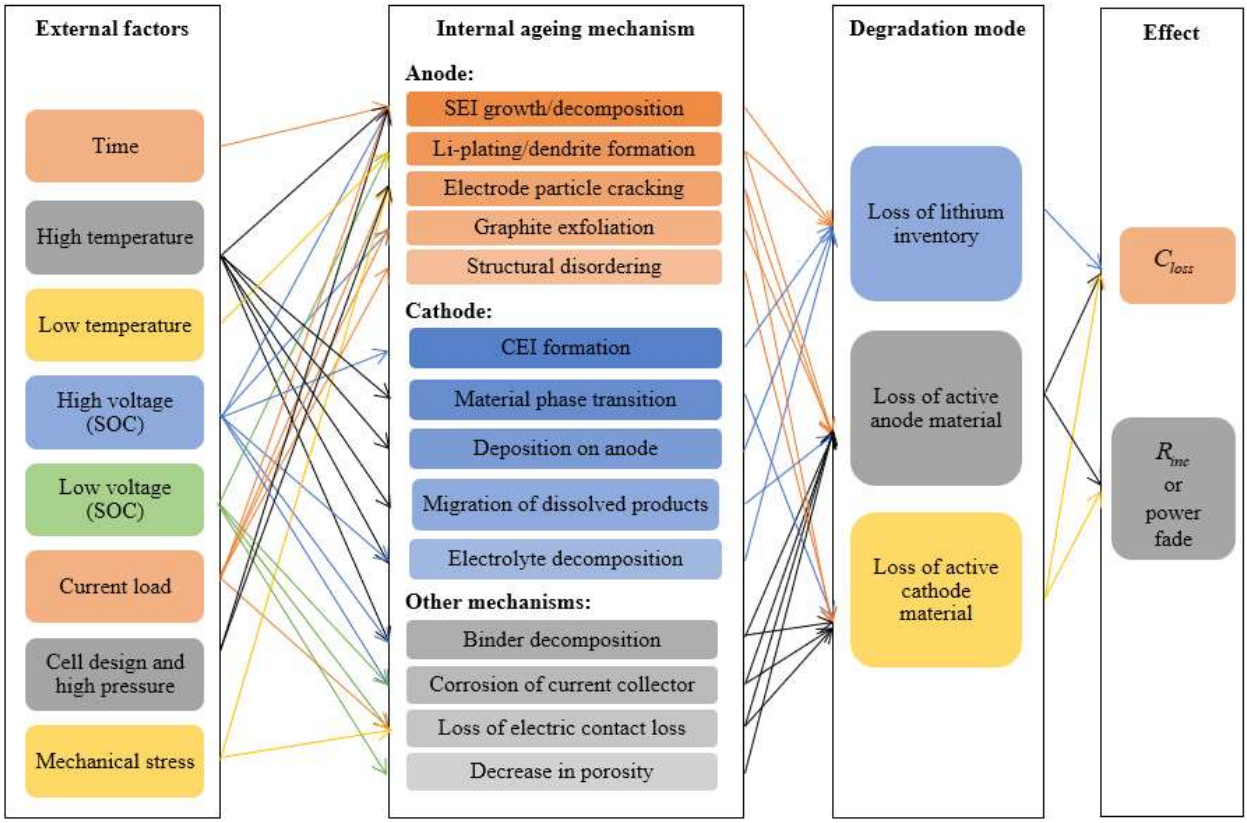

Figure 16. Cause and effect of degradation mechanisms adapted from *(98)*.

In the final step, we reviewed the recent advancement in SOH estimation methods integrated with internal degradation models and data-driven methods using artificial neural networks and deep learning. The comparison results for the SOH estimation approaches are presented in Table 6.

Table 6. A comparison of emerging SOH estimation methods.

Methods	Key benefits	Limitations
Data-driven approach	• Simple structure, • Easy to identify parameters and implementation, • Strong ability to consider nonlinearities, • High prediction accuracy,	• Easy to cause under-fitting problems due to its linear regression type • Potential overfitting problems • Poor generalization, long-term prediction, and uncertainty manageability

	• Robust to outliers, • Low prediction time.	• Performance highly depends on the training process.
Hybrid methods	• Prediction accuracy is high and avoids the estimation error from the model mismatch • Enhances the model's adaptability to varying operating conditions	• Computation is complicated and depends on experimental data • Restricts its applicability under more complex aging conditions when combined with model-based methods
Empirical methods	• Easy to be built up and quick to produce predictions • Simple structure easy of extracting model parameters, • Low computational effort	• Extensive laboratory tests over the entire operating range are required • Poor robustness and low accuracy, • difficulty in developing suitable laboratory aging tests to analyze the interaction between different aging processes and link them to life expectancy on an experimental basis • Low generalizability (restricted to a specific battery type and operating conditions).
Physics-based models	• High accuracy with an accurate model • linked to the underlying physics of the battery	• Heavy computation load for electrochemical modes • Challenging to obtain model parameters
DVA/ICA based methods	• Easy to monitor and implement in BMS for online applications • Indicative of the intercalation process.	• Limited to low current rates, sensitive to measurement noise and temperature, • Large data requirements of voltage and current measurements
Deep neural network	• Automates the feature learning process from the large amounts of data • Learn highly representative features that carry the most useful information of the data	• It needs a large amount of health data to train.

A few of the potential research directions suggested for the Li-ion battery research community to develop an intelligent battery management system are as follows:

- It is clear from the review that the modeling and estimation of the internal degradation processes are complex due to the interplay among these degradation mechanisms. Continuum models, which incorporate chemical/electrochemical kinetics and transport phenomena to produce more accurate predictions than empirical models, provide deeper insight into the cell. These models will offer a new perception of structural growth and the transport of ions in the SEI and need further research.
- These integrated model-based approaches, where the internal degradation models are combined with ECM or electrochemical models for SOH estimation, have significantly

improved SOH estimation accuracy but are still in an infant stage and an open area of future research.

- Integrating or reflecting the contributions of internal degradation mechanisms with empirical models could further improve the SOH estimation results and be another research direction.
- Incorporating varying-parameter ECMs for SOC and SOH estimation will further improve the estimation accuracy. The development of filters or learning schemes to estimate/learn the time-varying parameters can provide a more reliable prediction of SOH. However, estimating or learning the time-varying parameters in real-time is a challenging problem and could be an area of future research.
- A majority of the learning schemes are offline. The learning schemes must use the measured data in real-time to update the models with lesser computation requirements. This can be another potential area of research for developing real-time learning schemes for BMS.
- The hybrid approaches, which combine the model-based and data-driven approaches, are also promising areas of future research for the adaptability and autonomy of BMS in battery health prediction.

5.2 Findings from the SOH-coupled Model Validation (Task 2)

Our experimental model validation results showed good model accuracy with a root mean square error (RMSE) of 0.29 V. In addition, the numerical validation proved that the coupled model could represent the battery's life more accurately due to the incorporation of capacity fade in the ECM. The state estimation using EKF showed estimation accuracy ±1% for SOC, SOH, surface, and core temperature. A detailed experimental and numerical analysis of the findings are presented below.

5.2.1 Experimental Validation Results

The charge and discharge voltage and current data from the MACCOR host PC were exported to MATLAB to perform the validation. Figure 17 depicts the comparison results of the model voltage output with experimentally measured voltage. The model output tracks the experimentally obtained voltage under the same experimentally measured CC-CV input current over 52 charge and discharge cycles. The root mean square error was found to be 0.29 V. This implies the model represents the dynamics of the A123 26650 over the life-cycle of the battery accurately. Note that we have obtained experimental data for 52 cycles for analysis and are a reasonable number of cycles to generalize the result.

In the second step, we also evaluated the observability of the model via an EKF. We estimated the model states using the same CC-CV current measured experimentally. The results are shown in Figure 18. It can be clearly seen from Figure 18 that the EKF was able to estimate the model states (red lines) close to the experimental values. The SOC, SOH, and output voltage estimation errors are within a 1% band with RMSE 0.0108, 0.0157, and 0.3079, respectively. These results validate the analytical model proposed in the research and provide us the confidence to use them for fault detection discussed later in this section.

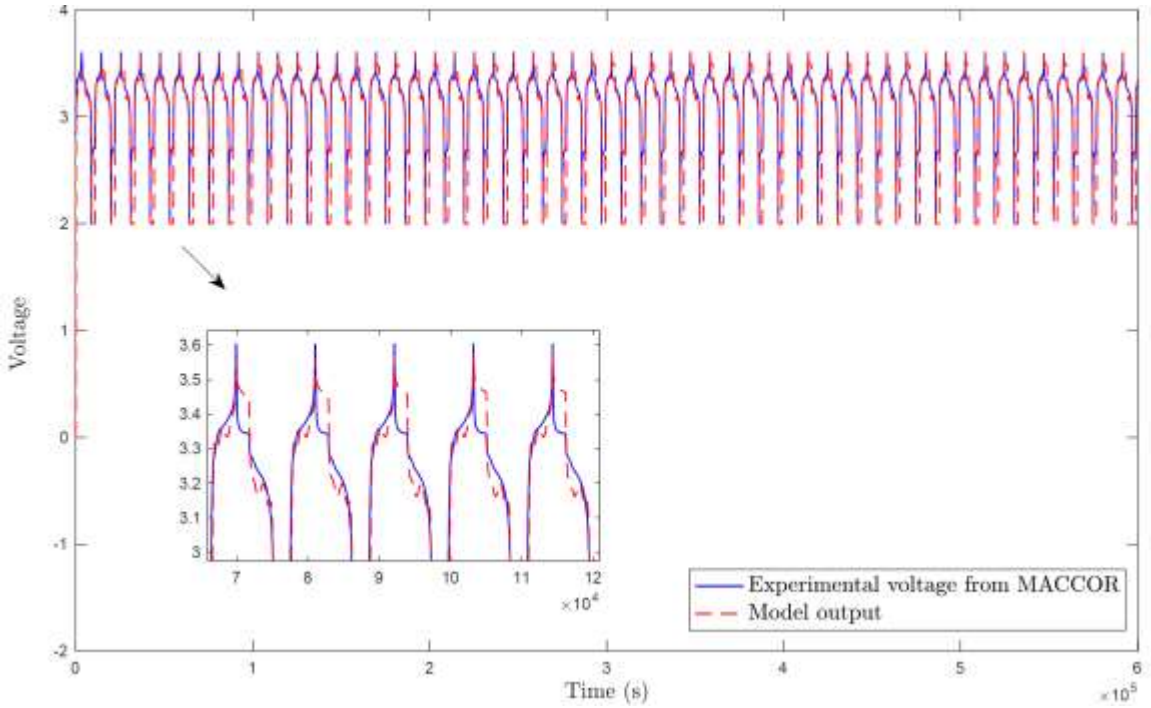

Figure 17. Comparison of the model output voltage with experimentally measured voltage for the A123 26650 LIB.

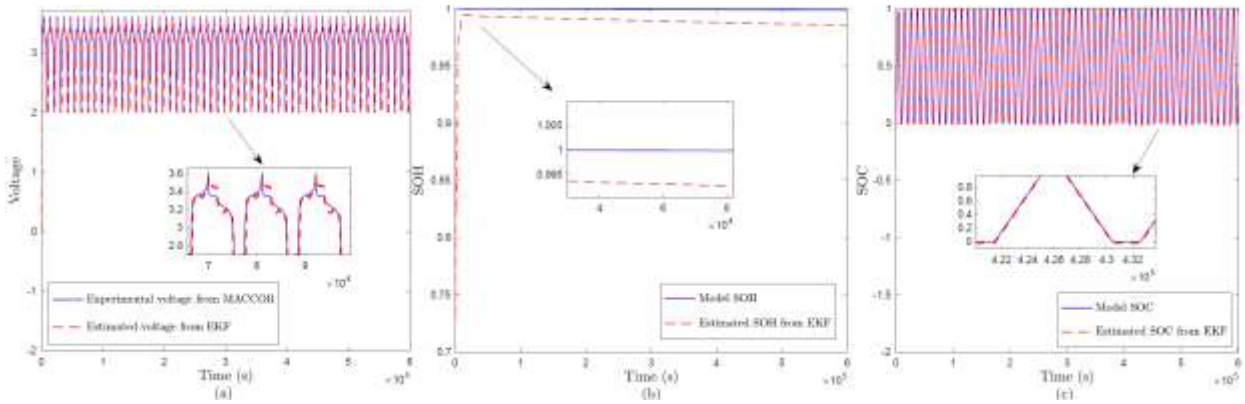

Figure 18. State estimation of the LIB using EKF and experimentally obtained charge-discharge current.

5.2.2 Findings from Simulation

To further investigate the model over the complete life-cycle of the LIB, we have conducted numerical simulations. We also have compared our results with the uncoupled modes available in the literature. The comparison results are shown in Figure 19. The results showed that the incorporation of the capacity fade when computing the SOC of the LIB leads to a more accurate estimation. Since SOC is the key to determining the driving range of an EV, the model will provide accurate range estimation over the battery's life and reduce the "range anxiety" significantly. A detailed analysis of the comparison is presented in the following few paragraphs.

In Figure 19 (a) and (b), the evolution of SOC for the proposed coupled model in Eq. (12) and the uncoupled model in *(101)* were compared. From Figure 19 (a), it can be seen that the SOCs during the first charge and discharge cycle are the same for both models. This is because the SOH value was 100% for both the models (initial value), and the initial conditions were kept the same

for a fair comparison. However, as the battery ages, the impact of SOH on SOC increases due to the change in C_{use}. Figure 19 (b) depicts both models' SOCcurves for a time window at approximate mid-life. It can be observed that although the time window for both the models is the same, the proposed coupled model was at its 2037th charge-discharge cycle, whereas the uncoupled model was at 2000th. As the battery's capacity fades, the C_{use} reduces, which leads to a shorter charging and discharging time for the coupled model. It makes the cell cycle more time within time. Since the uncoupled model does not account for the capacity fade, the charging time remains the same, leading to a lower cycle number in the same amount of time.

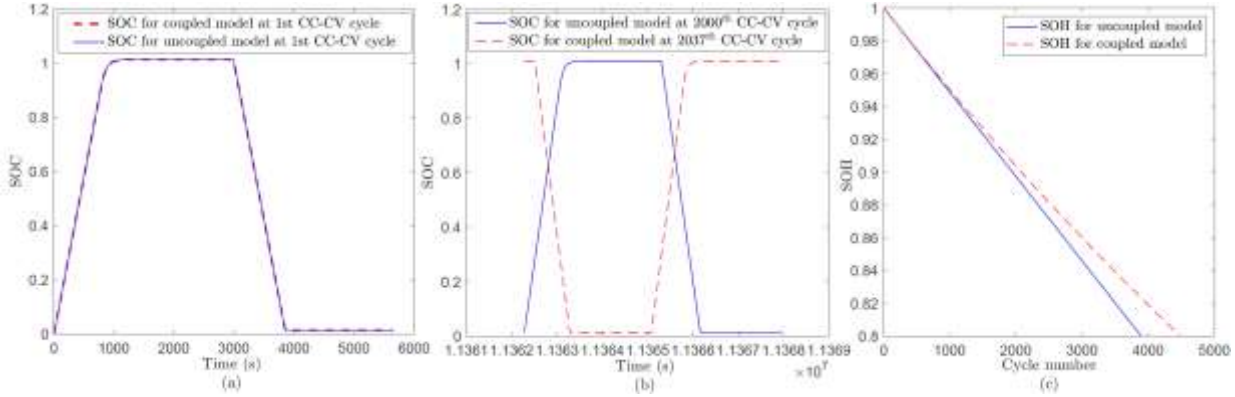

Figure 19. Comparison of (a) SOCs for the proposed SOH-coupled electro-thermal-aging model and SOH-uncoupled model for \$10 A (4.17 C_{rate}) $CC-CV$ cycles at $T_a = 25^0 C$, and (b) number of cycle numbers at the end of life (EOL).

It can be inferred that the use of the uncoupled models for SOC estimation and EV range calculation may lead to inaccurate results (higher or lower) after a certain period of use.

Further, Figure 19 (c) compares the SOH decays (capacity fade) to EOL (80%) for both models. It can be observed that the SOH for the uncoupled model decays to EOL with a lesser number of charge-discharge cycles than the proposed coupled model in Eq. (12). The EOL for the uncoupled model is achieved at 3887 cycles when compared to 4478 cycles for the proposed coupled model. This is as expected from the previous analysis. It can be further inferred that determining EOL using the uncoupled model may lead to erroneous perception of remaining useful life. In summary, the proposed coupled model is more accurate for SOC and SOH estimation when compared to the existing electro-thermal-aging models in *(101-102).*

5.3 Results and Finding from the Self-learning Model (Task 3)

The numerical validation found that the NN-based self-learning model can learn the nonlinear SOH-coupled model reasonably accurately. However, the error margins of the NN-based learning scheme are higher when compared to the EKF based approach. This is primarily due to two major challenges in online learning: 1) a limited number of measurements are available to train the NN weights (i.e., output feedback), and 2) hyper parameter tuning plays a critical role in the convergence of the NN weights. This requires further investigation in determining the architecture of the learning network, weight tuning rule, and hyper-parameter optimization. A detailed analysis is presented below.

The comparison results for the proposed reformulated model states and NN-based identifier states are shown in the following figures. Figure 20 compares the model voltage outputs with corresponding NN-based identifier outputs. It is clear that the NN-based identifier can estimate the SOH and terminal voltage close to the model output. However, the RMSE is higher than that of an EKF discussed in the previous section. Furthermore, it is observed that the NN could approximate the voltage within 1% in the first cycle with proper tuning of the learning gains (hyper-parameters).

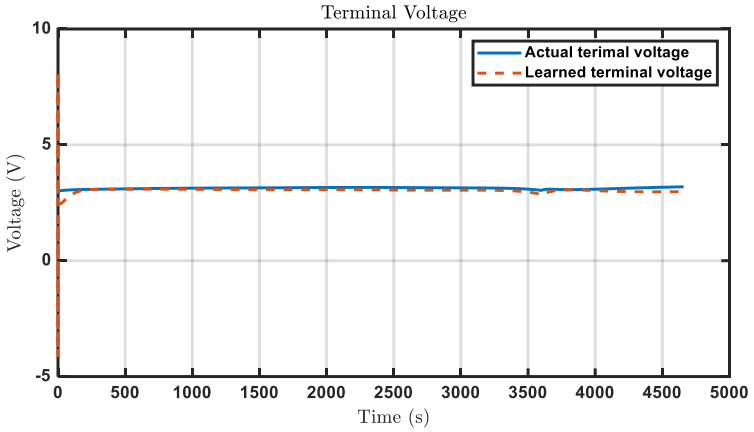

Figure 20. Comparison of SOH and the terminal voltage of the model and the NN-based identifier.

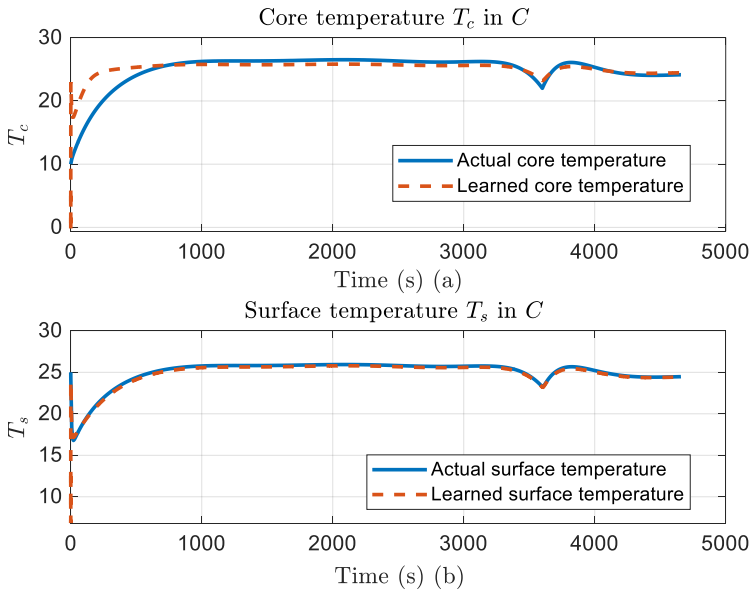

Figure 21. Comparison of surface and core temperature of the model and the NN-based identifier.

On the other hand, it was observed that the surface and core temperatures, shown in Figure 21, were learned with great accuracy. However, the SOC and SOH estimation results were found to have a larger error, as shown in Figure 22. Note that the comparison results are over two charge-discharge cycles. It was further observed that by tuning the hyper-parameters (NN learning gains), the estimation accuracy could be improved for one cycle. However, to generalize over the life-cycle of the LIB is a challenging task. This requires further investigation for the NN architecture and tuning rule for the weights. It is worth mentioning that the NN weights were tuned online with

real-time measurement, and there were no target values as in the case of offline traditional machine learning algorithms. This makes the problem further challenging and requires further investigation.

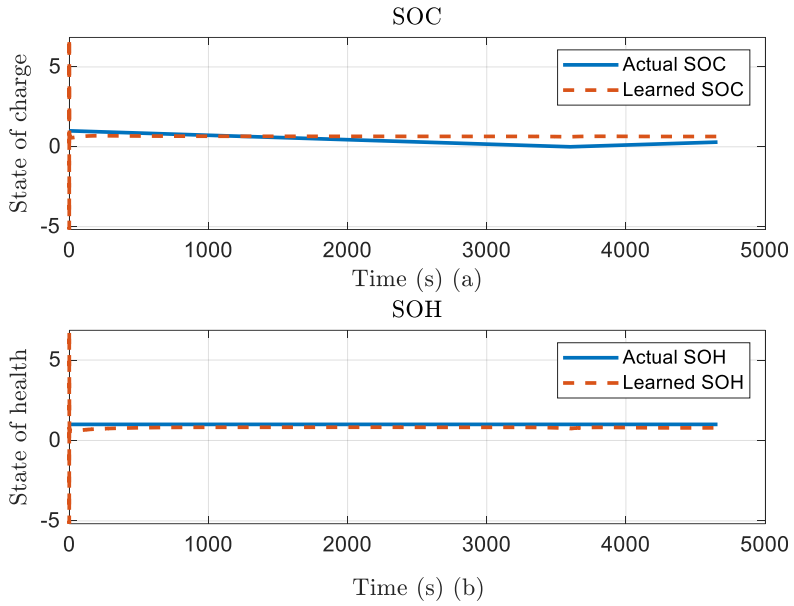

Figure 22. Comparison of SOC and SOH of the model and the NN-based identifier.

5.4 Results and Finding from the Fault Detection Scheme (Task 4)

In this section, we preset the analysis and finding for the fault detection scheme using the reformulated model in Eq. (24). It is found that the reformulated model can estimate the states (SOC, SOH, surface, and core temperature) and the internal resistance of the battery more accurately. Since the most critical fault in a LIB is the thermal fault, the variation in internal resistance, core, and surface temperature can be used to isolate the onset of the internal temperature rise. Due to the higher RMSE of the NN-based self-learning identifier, we have used an EKF as the fault detection observer to develop the model-based detection scheme. In the following, a detailed analysis of the effectiveness of the EKF for fault analysis is presented.

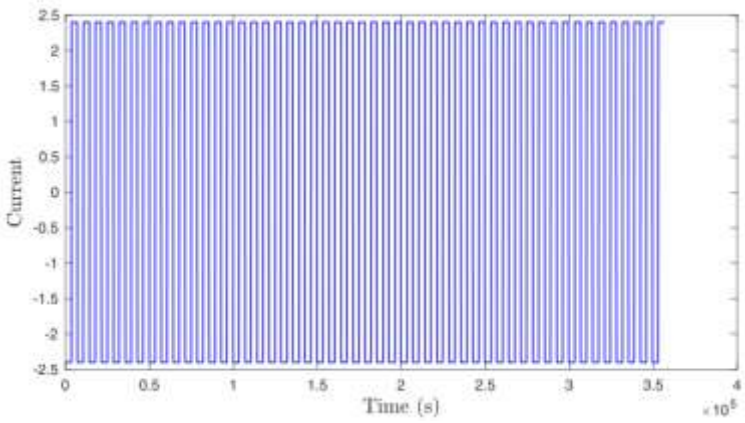

Figure 23. Input current without rest condition in amperes at 1 C-rate

First, we have analyzed the EKF estimation accuracy under the charge/discharge cycle at $1C_{rate}$ without the rest period, as shown in Figure 23. The estimated parameter R_0 , along with estimated states, are shown in Figure 24. The estimation results are shown for 50 charge/discharge cycles. It can be observed that the estimation errors for states SOC, T_c , R_0 and SOH in Figure 24 (a), (b), (c), and (d), respectively, converge close to the actual values proving that the proposed coupled model can be used to design an EKF which can simultaneously estimate the state and internal resistance of LIB. Furthermore, the R_0 and output voltage estimation error for charge/discharge input are within a 1% band with RMSE's 0.0034, and 0.0072, respectively.

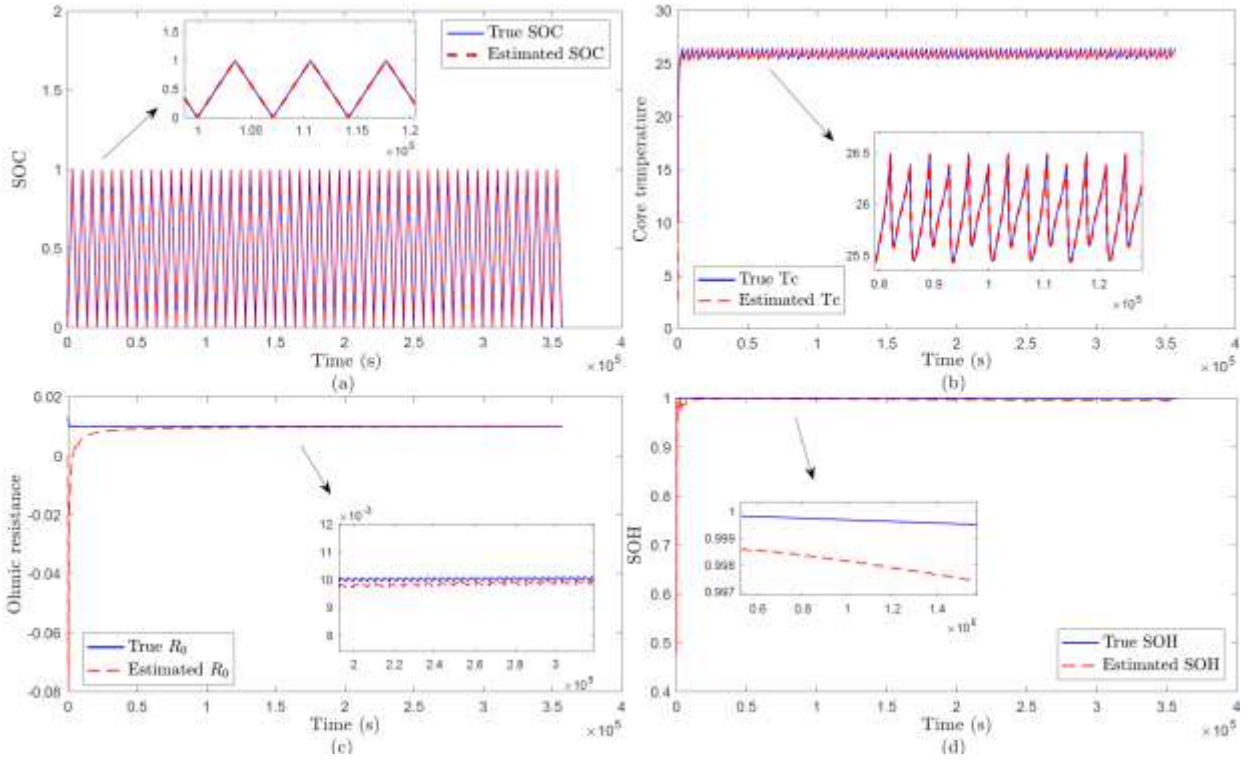

Figure 24 Simultaneous state and internal resistance estimation of the reformulated model using EKF under 1C charge and discharge current

Upon successful results from the EKF based state estimator, we validated the model-based fault detection scheme using the EKF as a detection observer. It can be seen from Figure 25 (d) that the output residual increases with the software fault incorporated in the model at the time of 30,000 seconds. The residual is larger and beyond the threshold in the initial estimation phase of the EKF. Therefore, the detection algorithm is not activated during the initial estimation phase to avoid false positives. Once the state estimation error converges, the detection algorithm is activated to monitor the residual. It is clear from the simulation that the terminal voltage can be used to detect the fault. Note that the simulation results shown in Figure 25 is over 200 charge-discharge cycles. Therefore, the residuals look noisy.

To isolate the fault, we also have plotted the residuals for the surface temperature (Figure 25 (a)), core temperature (Figure 25(b)), and internal resistance (Figure 25 (c)). All the residuals increase since all these states are affected by the internal temperature rise. It can be further noticed

that the core temperature rises at a faster rate when compared to other ones, implying a core temperature rise. This validated the fault detection scheme.

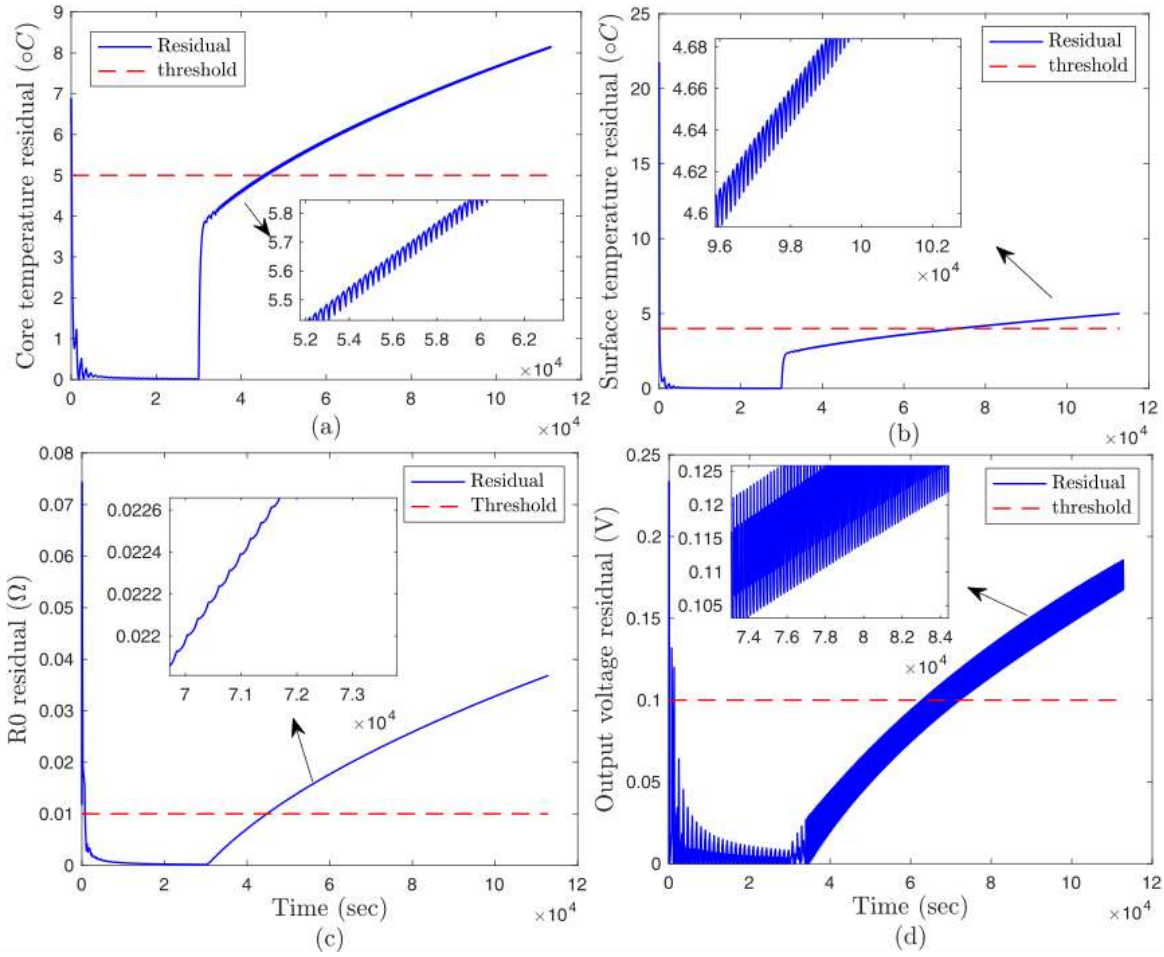

Figure 25. Residual generation and fault detection and isolation.

It is clear from the results that the proposed coupled model can be used to develop an EKF based fault detection observer. The SOH-coupling and reformulation to incorporate internal resistance as a state can help isolate the fault by monitoring all the states simultaneously. Note that the thresholds used for the fault detection are constant. However, since the model incorporates SOH and parameter variation with degradation, the threshold can be designed to be adaptive and need further investigation. Implementing the fault detection scheme on board BMS will significantly improve the safety of EVs from thermal runaway. The proposed scheme requires further experimental evaluation using use-cases prior to implementation.

6. CONCLUSIONS

This project has extensively reviewed the literature and developed SOH-coupled models and a model-based fault detection scheme. The review concluded that SOH estimation is a complex and challenging task due to the correlation between the internal and external factors and the degradation mechanisms. Nondestructive quantitative evaluations of the degradation, taking the impact of aging factors (increment in internal resistance, increase in Li-plating, LLI, and operating conditions) into account, will result in a more accurate estimation of the health of the battery and longer life.

The proposed SOH-coupled models can simultaneously estimate the SOC and SOH and can be used for fault and stress detection. The model validation results showed that the models represent the battery dynamics more accurately when compared to the uncoupled models throughout the LIB's life. The EKF based state estimation under different current profiles further exemplifies the model behavior in representing the life-cycle of the battery. It can be further concluded that the self-learning algorithm using the NNs can learn the model with reasonable accuracy. However, the accuracy is less than the EKF. This is because online training of the NN weights with limited measurements leads to a higher approximation error. This requires further investigation for tuning of the hyperparameters for training. Finally, incorporating the internal resistance as a state of the model enables the estimation of this parameter using an EKF. This further helps in detecting and isolating internal faults.

In summary, the SOH-coupled models can produce more accurate results in SOC and SOH estimation and fault detection and isolation. The development of real-time machine learning schemes with measured voltage, current, and surface temperature can address the challenges in modeling the internal degradation by leveraging the advancement in NN-based architectures and training schemes. Further, these learning-based intelligent models can be implemented in BMS for health-conscious decision-making with improved autonomy. The analytical results need to be further validated using use-cases and onboard EVs for implementation on board BMS.

REFERENCES

1. *Sales of plug-in electric vehicles in the US 2018 Statista.* [Online]. Available: https://www.statista.com/statistics/416672/united-states-projected-plug-in-electric-vehicles-sales/.
2. *Press Release: Federal Highway Administration Unveils National 'Alternative Fuel and Electric Charging' Network, 11/3/2016 | Federal Highway Administration.* [Online]. Available: https://www.fhwa.dot.gov/pressroom/fhwa1656.cfm.
3. *Global EV Outlook 2019 – Analysis - IEA.* [Online]. Available: https://www.iea.org/reports/global-ev-outlook-2019.
4. Lithium Ion Battery Market Share will Reach US $92 Billion by 2024. *Marketwatch*, Apr. 2019.
5. Abada, S., Marlair, G., Lecocq, A., Petit, M., Sauvant-Moynot, V., and Huet, F. Safety focused modeling of lithium-ion batteries: A review. *J. Power Sources*, 2016. 306:178–192.
6. Pattipati, Bharath, Krishna Pattipati, Jon P. Christopherson, Setu Madhavi Namburu, Danil V. Prokhorov, and Liu Qiao. Automotive battery management systems. *IEEE*, 2008.
7. Conte, F. V. Battery and battery management for hybrid electric vehicles: A review. *Elektrotechnik and Informationstechnik*, 2006. 123(10): 424–431.
8. Srinivasan, V. and Wang, C. Y. Analysis of electrochemical and thermal behavior of Li-ion cells. *J. Electrochem. Soc.*, vol. 150, no. 1, pp. A98--A106, 2003.
9. Doyle, M., Fuller, T. F. and Newman, J. Modeling of galvanostatic charge and discharge of the lithium/polymer/insertion cell. *J. Electrochem. Soc.*, 1993. 140(6): 1526–1533.
10. Fuller, T. F., Doyle, M., and Newman, J., Simulation and optimization of the dual lithium-ion insertion cell. *J. Electrochem. Soc. 1994.*141(1): 1–10.
11. Hu, Xiaosong, Shengbo Li, and Huei Peng. A comparative study of equivalent circuit models for Li-ion batteries. *J. Power Sources*, 2012. 198: 359–367.
12. Nejad, S., Gladwin, D. T., and Stone, D. A., A systematic review of lumped-parameter equivalent circuit models for real-time estimation of lithium-ion battery states. *J. Power Sources, 2016.* 316: 183–196.
13. Fleischer, C., Waag, W., Heyn, H.-M., and Sauer, D. U. Online adaptive battery impedance parameter and state estimation considering physical principles in reduced order equivalent circuit battery models: Part 1. Requirements, critical review of methods and modeling. *J. Power Sources*, 2014. 260: 276–291.
14. Benini, L., Castelli, G., Macii, A., Macii, E., Poncino, M., and Scarsi, R., Discrete-time battery models for system-level low-power design. *IEEE Trans. Very Large Scale Integr. Syst.*, 2001. 5: 630–640.
15. Chen M., and Rincon-Mora, G. A. Accurate electrical battery model capable of predicting run-time and IV performance. *IEEE Trans. Energy Convers.*, 2006. 21: 504–511.
16. Weng, C., Cui, Y., Sun, J., and Peng, H. On-board state of health monitoring of lithium-ion batteries using incremental capacity analysis with support vector regression. *J. Power Sources*, 2013. 235: 36–44.
17. You, G., Park, G., and Oh, D. Real-time state-of-health estimation for electric vehicle batteries: A data-driven approach. *Appl. Energy*, 2016. 176: 92–103.

18. Pola D. A., *et al.*, Particle-filtering-based discharge time prognosis for lithium-ion batteries with a statistical characterization of use profiles. *IEEE Trans. Reliab.*, 2015. 64 (2): 710–720.
19. Liu, D., Pang, J., Zhou, J., Peng, Y., and Pecht, M. Prognostics for state of health estimation of lithium-ion batteries based on combination Gaussian process functional regression. *Microelectron. Reliab.*, 2013. 53: 832–839.
20. He, H., Xiong, R., and Fan, J., Evaluation of lithium-ion battery equivalent circuit models for state of charge estimation by an experimental approach. *Energies*, 2011. 4: 582–598.
21. Xiong, Rui, F-C. Sun, and H-W. He. Data-driven state-of-charge estimator for electric vehicles battery using robust extended Kalman filter. *Int. J. Automot. Technol.*, 2014. 15: 89–96.
22. Krewer, Ulrike, Fridolin Röder, Eranda Harinath, Richard D. Braatz, Benjamin Bedürftig, and Rolf Findeisen. Review-Dynamic Models of Li-Ion Batteries for Diagnosis and Operation: A Review and Perspective. *Journal of the electrochemical society, 2018.* 165: pp. A3656–A3673.
23. Srinivasan, Venkat, and C. Y. Wang. Analysis of electrochemical and thermal behavior of Li-ion cells. *J. Electrochem. Soc.*, 2003. 150: A98--A106.
24. Ren, Hongbin, Yuzhuang Zhao, Sizhong Chen, and Taipeng Wang. Design and implementation of a battery management system with active charge balance based on the SOC and SOH online estimation. *Energy*, 2019. 166: 908–917.
25. Moura, Scott J., Nalin A. Chaturvedi, and Miroslav Krstic. PDE estimation techniques for advanced battery management systems—Part II: SOH identification. *American Control Conference (ACC)*, 2012. 566–571.
26. Li, Jiahao, Joaquin Klee Barillas, Clemens Guenther, and Michael A. Danzer. A comparative study of state of charge estimation algorithms for LiFePO4 batteries used in electric vehicles. *Journal of power sources*, 2013. 230: 244–250.
27. Waag, Wladislaw, Christian Fleischer, and Dirk Uwe Sauer. Critical review of the methods for monitoring of lithium-ion batteries in electric and hybrid vehicles. *Journal of Power Sources*, 2014. 258: 321–339.
28. Lin, Cheng, Aihua Tang, and Wenwei Wang. A review of SOH estimation methods in lithium-ion batteries for electric vehicle applications. *Energy Procedia*, 2015. 75: 1920–1925.
29. Vennam, G. and Sahoo, A. Simultaneous state and parameter estimation of lithium-ion battery: An observer based approach. *AmericanControl Conference* (ACC), 2019. 4485–4490.
30. Plett, Gregory L. Extended Kalman filtering for battery management systems of LiPB-based HEV battery packs: Part 3. state and parameter estimation. *Journal of Power sources*, 2004. 134: 277–292.
31. Lu, Languang, Xuebing Han, Jianqiu Li, Jianfeng Hua, and Minggao Ouyang. A review on the keyissues for lithium-ion battery management in electric vehicles. *Journalof power sources*, 2013. 226: 272–288.
32. Heinrich, Marco, Nicolas Wolff, Nina Harting, Vincent Laue, Fridolin Röder, Steffen Seitz, and Ulrike Krewer. Physico-chemical modeling of a lithium-ion battery: an ageing study with electrochemical impedance spectroscopy. *Batteries& Supercaps*, 2019. 2: 530–540.

33. Wang, John, Ping Liu, Jocelyn Hicks-Garner, Elena Sherman, Souren Soukiazian, Mark Verbrugge, Harshad Tataria, James Musser, and Peter Finamore. Cycle-life modelfor graphite-lifepo4 cells. *Journal of Power Sources*, 2011. 196: 3942–3948.
34. Lin, Xinfan, Hector E. Perez, Shankar Mohan, Jason B. Siegel, Anna G. Stefanopoulou, Yi Ding, and Matthew P. Castanier. A lumped-parameter electro-thermalmodel for cylindrical batteries. *Journal of Power Sources*, 2014. 257: 1–11.
35. Perez, Hector Eduardo, Xiaosong Hu, Satadru Dey, and Scott J. Moura. "Optimal charging of li-ion batteries with coupled electro-thermal-aging dynamics. *IEEE Transactions on Vehicular Technology*, 2017. 66: 7761–7770.
36. Pang, Hui, Long Guo, Longxing Wu, Jiamin Jin, Fengqi Zhang, and Kai Liu. A novel extended Kalman filter-based battery internal and surface temperature estimation based on an improved electro-thermal model. *Journal of Energy Storage*, 2021. 41: 102854.
37. Suri, Girish, and Simona Onori. A control-oriented cycle-life model for hybrid electric vehicle lithium-ion batteries. *Energy*, 2016. 96: 644–653.
38. Liu, Kailong, Changfu Zou, Kang Li, and Torsten Wik. Charging pattern optimization for lithium-ion batteries with an electrothermal-aging model. *IEEE Transactions on Industrial Informatics*, 2018. 14: 5463–5474.
39. Hashemi, Seyed Reza, Ajay Mohan Mahajan, and Siamak Farhad. Online estimationof battery model parameters and state of health in electric and hybrid aircraft application. *Energy*, 2021. 229: 120699.
40. Yuan, Shifei, Hongjie Wu, and Chengliang Yin. State of charge estimation using the extended Kalman filter for battery management systems based on the ARX battery model. *Energies*, 2013. 6: 444–470.
41. Dey, Satadru, Beshah Ayalew, and Pierluigi Pisu. Nonlinear robust observers for state-of-charge estimation of lithium-ion cells based on a reduced electrochemical model. *IEEE Trans. Control Syst. Technol.*, 2015, 23: 1935–1942.
42. Tang, Xidong, Xiaofeng Mao, Jian Lin, and Brian Koch. Li-ion battery parameter estimation for state of charge. *American Control Conference* (ACC), 2011. 941–946.
43. Li, Jiahao, *Joaquin* Klee Barillas, Clemens Guenther, and Michael A. Danzer. A comparative study of state of charge estimation algorithms for LiFePO4 batteries used in electric vehicles. *J. Power Sources*, 2013. 230: 244–250.
44. Lipu, Molla S. Hossain, Mahammad A. Hannan, Aini Hussain, Mohamad HM Saad, Afida Ayob, and Frede Blaabjerg. State of Charge Estimation for Lithium-ion Battery Using Recurrent NARX Neural Network Model Based Lighting Search Algorithm. *IEEE Access*, 2018. 6: 28150–28161.
45. Xia, Bizhong, Deyu Cui, Zhen Sun, Zizhou Lao, Ruifeng Zhang, Wei Wang, Wei Sun, Yongzhi Lai, and Mingwang Wang. State of charge estimation of lithium-ion batteries using optimized Levenberg-Marquardt wavelet neural network. *Energy*, 2018. 153: 694–705.
46. Chemali, Ephrem, Phillip J. Kollmeyer, Matthias Preindl, Ryan Ahmed, and Ali Emadi. Long short-term memory networks for accurate state-of-charge estimation of Li-ion batteries. *IEEE Trans. Ind. Electron.*, 2018. 65: 6730–6739.
47. Dubarry, Matthieu, Vojtech Svoboda, Ruey Hwu, and Bor Yann Liaw. Capacity loss in rechargeable lithium cells during cycle life testing: The importance of determining state-of-

charge. *J. Power Sources*, 2007. 174: 1121–1125.
48. Andre, Dave, Christian Appel, Thomas Soczka-Guth, and Dirk Uwe Sauer. Advanced mathematical methods of SOC and SOH estimation for lithium-ion batteries. *J. Power Sources*, 2013. 224: 20–27.
49. Marcicki, James, Marcello Canova, A. Terrence Conlisk, and Giorgio Rizzoni. Design and parametrization analysis of a reduced-order electrochemical model of graphite/LiFePO4 cells for SOC/SOH estimation. *J. Power Sources*, 2013. 237: 310–324.
50. Feng, Xuning, Jianqiu Li, Minggao Ouyang, Languang Lu, Jianjun Li, and Xiangming He. Using probability density function to evaluate the state of health of lithium-ion batteries. *J. Power Sources*, 2013. 232: 209–218.
51. Schmalstieg, Johannes, Stefan Käbitz, Madeleine Ecker, and Dirk Uwe Sauer. A holistic aging model for Li (NiMnCo) O2 based 18650 lithium-ion batteries. *J. Power Sources*, vol. 257, pp. 325–334, 2014.
52. Baccouche, Ines, Sabeur Jemmali, Bilal Manai, Noshin Omar, and Najoua Essoukri Ben Amara. Improved OCV model of a Li-ion NMC battery for online SOC estimation using the extended Kalman filter. *Energies*, 2017. 10: 764.
53. Di Domenico, Domenico, Giovanni Fiengo, and Anna Stefanopoulou. Lithium-ion battery state of charge estimation with a Kalman filter based on a electrochemical model. *Control Applications*, 2008. 702–707.
54. He, Wei, Nicholas Williard, Chaochao Chen, and Michael Pecht. State of charge estimation for electric vehicle batteries using unscented Kalman filtering. *Microelectron. Reliab.*, 2013. 53: 840–847.
55. Tian, Yong, Bizhong Xia, Wei Sun, Zhihui Xu, and Weiwei Zheng. A modified model based state of charge estimation of power lithium-ion batteries using unscented Kalman filter. *J. Power Sources*, 2014. 270: 619–626.
56. Sun, Fengchun, Xiaosong Hu, Yuan Zou, and Siguang Li. Adaptive unscented Kalman filtering for state of charge estimation of a lithium-ion battery for electric vehicles. *Energy*, 2011. 36: 3531–3540.
57. Sepasi, Saeed, Reza Ghorbani, and Bor Yann Liaw. Improved extended Kalman filter for state of charge estimation of battery pack. *J. Power Sources*, 2014. 255: 368–376.
58. Dey, Satadru, B. Ayalew, and P. Pisu. Nonlinear adaptive observer for a lithium-ion battery cell based on coupled electrochemical--thermal model. *J. Dyn. Syst. Meas. Control*, 2015. 137: 111005.
59. Xia, Bizhong, Chaoren Chen, Yong Tian, Wei Sun, Zhihui Xu, and Weiwei Zheng. A novel method for state of charge estimation of lithium-ion batteries using a nonlinear observer. *J. Power Sources*, 2014. 270: 359–366.
60. Chen, Wen, Wei-Tian Chen, Mehrdad Saif, Meng-Feng Li, and Hai Wu. Simultaneous fault isolation and estimation of lithium-ion batteries via synthesized design of Luenberger and learning observers. *IEEE Trans. Control Syst. Technol.*, 2014. 22: 290–298.
61. Li, Weilin, Liliuyuan Liang, Wenjie Liu, and Xiaohua Wu. State of charge estimation of lithium-ion batteries using a discrete-time nonlinear observer. *IEEE Trans. Ind. Electron.*, 2017. 64: 8557–8565.
62. Hu, Xiaosong, Fengchun Sun, and Yuan Zou. Estimation of state of charge of a lithium-ion

battery pack for electric vehicles using an adaptive Luenberger observer. *Energies*, 2010. 3: 1586–1603.
63. Wei, Zhongbao, Changfu Zou, Feng Leng, Boon Hee Soong, and King-Jet Tseng. Online model identification and state-of-charge estimate for lithium-ion battery with a recursive total least squares-based observer. *IEEE Trans. Ind. Electron*., 2018. 65: 1336–1346.
64. Afshar, Sepideh, Kirsten Morris, and Amir Khajepour. State-of-Charge Estimation Using an EKF-Based Adaptive Observer. *IEEE Trans. Control Syst. Technol*., 2018. 99: 1–17.
65. Kim, IL-Song. A technique for estimating the state of health of lithium batteries through a dual-sliding-mode observer. *IEEE Trans. Power Electron*., 2010. 25: 1013–1022.
66. Charkhgard, Mohammad, and Mohammad Farrokhi. State-of-charge estimation for lithium-ion batteries using neural networks and EKF. *IEEE Trans. Ind. Electron*., 2010. 57: 4178–4187.
67. Shen, Y. Adaptive online state-of-charge determination based on neuro-controller and neural network. *Energy Convers. Manag*., 2010. 51: 1093–1098.
68. He, Wei, Nicholas Williard, Chaochao Chen, and Michael Pecht. State of charge estimation for Li-ion batteries using neural network modeling and unscented Kalman filter-based error cancellation. *Int. J. Electr. Power Energy Syst.*, 2014. 62: 783–791.
69. Chen, Jian, Quan Ouyang, Chenfeng Xu, and Hongye Su. Neural network-based state of charge observer design for lithium-ion batteries. *IEEE Trans. Control Syst. Technol*., 2018. 26: 313–320.
70. Hannan, Mahammad A., Molla S. Hossain Lipu, Aini Hussain, Mohamad H. Saad, and Afida Ayob. "Neural network approach for estimating state of charge of lithium-ion battery using backtracking search algorithm. *IEEE Access*, 2018. 6: 10069–10079.
71. Gao, Lijun, Shengyi Liu, and Roger A. Dougal. Dynamic lithium-ion battery model for system simulation. *IEEE Trans. components Packag*. Technol., 2002. 25: 495–505.
72. Plett, G. L. Extended Kalman filtering for battery management systems of LiPB-based HEV battery packs: Part 3. State and parameter estimation. *J. Power Sources*, 2004. 134: 277–292.
73. Dai, Haifeng, Xuezhe Wei, and Zechang Sun. State and parameter estimation of a HEV Li-ion battery pack using adaptive Kalman filter with a new SOC-OCV concept. *International Conference on Measuring Technology and Mechatronics Automation*, 2009, 2: 375–380.
74. Partovibakhsh, Maral, and Guangjun Liu. An adaptive unscented Kalman filtering approach for online estimation of model parameters and state-of-charge of lithium-ion batteries for autonomous mobile robots. *IEEE Trans. Control Syst. Technol*., 2015. 23: 357–363.
75. Biswas, Atriya, Ran Gu, Phil Kollmeyer, Ryan Ahmed, and Ali Emadi. Simultaneous State and Parameter Estimation of Li-Ion Battery With One State Hysteresis Model Using Augmented Unscented Kalman Filter. *IEEE Transportation Electrification Conference and Expo* (ITEC), 2018. 1065–1070.
76. Spotnitz, R., and J. Franklin. Abuse behavior of high-power lithium-ion cells. *J. Power Sources*, 2003. 113: 81–100.
77. Marcicki, Jim, Simona Onori, and Giorgio Rizzoni. Nonlinear fault detection and isolation for a lithium-ion battery management system. *ASME Dynamic Systems and Control Conference*, 2010. 607–614.
78. Dey, Satadru, Sara Mohon, Pierluigi Pisu, and Beshah Ayalew. Sensor fault detection,

isolation, and estimation in lithium-ion batteries," *IEEE Trans. Control Syst. Technol*., 2016. 24: 2141–2149.
79. Liu, Zhentong, and Hongwen He. Sensor fault detection and isolation for a lithium-ion battery pack in electric vehicles using adaptive extended Kalman filter. *Appl. Energy,* 2017. 185: 2033–2044.
80. Sidhu, Amardeep, Afshin Izadian, and Sohel Anwar. Adaptive nonlinear model-based fault diagnosis of Li-ion batteries. *IEEE Trans. Ind. Electron*., 2015. 62: 1002–1011.
81. Dey, Satadru, and Beshah Ayalew. A diagnostic scheme for detection, isolation and estimation of electrochemical faults in lithium-ion cells. *ASME Dynamic Systems and Control Conference,* 2015.
82. Miao, Qiang, Lei Xie, Hengjuan Cui, Wei Liang, and Michael Pecht. Remaining useful life prediction of lithium-ion battery with unscented particle filter technique. *Microelectron. Reliab*., 2013. 53: 805–810.
83. Ferdowsi, Hasan, and Sarangapani Jagannathan. Fault diagnosis of a class of distributed parameter systems modeled by parabolic partial differential equations. *American Control Conference* (ACC), 2014. 5434–5439.
84. Singh, Amardeep, Afshin Izadian, and Sohel Anwar. Nonlinear model based fault detection of lithium-ion battery using multiple model adaptive estimation. *IFAC Proc*. 2014. 47: 8546–8551.
85. Hannan, Mohammad A., MS Hossain Lipu, Aini Hussain, and Azah Mohamed. A review of lithium-ion battery state of charge estimation and management system in electric vehicle applications: Challenges and recommendations*," Renewable and Sustainable Energy Reviews*, 2017. 78: 834–854
86. Lu, Languang, Xuebing Han, Jianqiu Li, Jianfeng Hua, and Minggao Ouyang. A review on the key issues for lithium-ion battery management in electric vehicles. *Journal of power sources*, 2013. 226: 272–288.
87. Xia, Bing, Yunlong Shang, Truong Nguyen, and Chris Mi. A correlation based fault detection method for short circuits in battery packs. *Journal of Power Sources*, 2017. 337: 1–10.
88. Xia, Bing, Zheng Chen, Chris Mi, and Brian Robert. External short circuit fault diagnosis for lithium-ion batteries. Transportation Electrification Conference and Expo (ITEC), 2014. 1–7.
89. Gao, Zhiwei, Carlo Cecati, and Steven X. Ding. A survey of fault diagnosis and fault-tolerant techniques—part i: Fault diagnosis with model-based and signal-based approaches. IEEE Transactions on Industrial Electronics, 2015. 62: 3757–3767.
90. Dey, Satadru, Hector E. Perez, and Scott J. Moura. Model-based battery thermal fault diagnostics: Algorithms, analysis, and experiments. *IEEE Transactions on Control Systems Technology*, 2017. 99: 1–12.
91. Liu, Zhentong, and Hongwen He. Sensor fault detection and isolation for a lithium-ion battery pack in electric vehicles using adaptive extended Kalman filter. *Applied Energy*, 2017. 185: 2033–2044.
92. Sidhu, Amardeep, Afshin Izadian, and Sohel Anwar. Adaptive nonlinear model-based fault diagnosis of li-ion batteries. *IEEE Transactions on Industrial Electronics*,2015. 62: 1002–1011.

93. Dey, Satadru, and Beshah Ayalew. A diagnostic scheme for detection, isolation and estimation of electrochemical faults in lithium-ion cells. in *ASME 2015 Dynamic Systems and Control Conference*, 2015.
94. Zheng, Changwen, Yunlong Ge, Ziqiang Chen, Deyang Huang, Jian Liu, and Shiyao Zhou. Diagnosis method for li-ion battery fault based on an adaptive unscented Kalman filter," *Energies*, 2017. 10: 1810.
95. Ferdowsi, Hasan, and Sarangapani Jagannathan. Fault diagnosis of a class of distributed parameter systems modeled by parabolic partial differential equations. *American Control Conference* (ACC), 2014. 5434–5439.
96. Chen, Wen, Wei-Tian Chen, Mehrdad Saif, Meng-Feng Li, and Hai Wu. Simultaneous fault isolation and estimation of lithium-ion batteries via synthesized design of Luenberger and learning observers. *IEEE Transactions on Control Systems Technology*, 2014. 22: 290–298.
97. Singh, Amardeep, Afshin Izadian, and Sohel Anwar. Fault diagnosis of li-ion batteries using multiple-model adaptive estimation. in *Industrial Electronics Society*, 2013. 3524–3529.
98. Birkl CR, Roberts MR, McTurk E, Bruce PG, Howey DA. Degradation diagnostics for lithium ion cells. *Journal of Power Sources*, 2017. 341: 373–86.
99. Heinrich M, Wolff N, Harting N, Laue V, R¨oder F, Seitz S, et al. Physico-chemical modeling of a lithium-ion battery: an ageing study with electrochemical impedance spectroscopy. *Batteries & Supercaps*, 2019. 2: 530–40.
100. Perez, Hector E., Jason B. Siegel, Xinfan Lin, Anna G. Stefanopoulou, Yi Ding, and Matthew P. Castanier. Parameterization and validation of an integrated electro-thermal cylindrical LFP battery model. *Dynamic Systems and Control Conference*, 2012. 45318: 41–50.
101. Pang, Hui, Long Guo, Longxing Wu, Jiamin Jin, Fengqi Zhang, and Kai Liu. A novel extended Kalman filter-based battery internal and surface temperature estimation based on an improved electro-thermal model. *Journal of Energy Storage*, 2021. 41: 102854.
102. Perez, Hector Eduardo, Xiaosong Hu, Satadru Dey, and Scott J. Moura. Optimal charging of li-ion batteries with coupled electro-thermal-aging dynamics. *IEEE Transactions on Vehicular Technology*, 2017. 66: 7761–7770.
103. Suri, Girish, and Simona Onori. A control-oriented cycle-life model for hybrid electric vehicle lithium-ion batteries. *Energy*, 2016. 96: 644–653.
104. Lin, Xinfan, Hector E. Perez, Shankar Mohan, Jason B. Siegel, Anna G. Stefanopoulou, Yi Ding, and Matthew P. Castanier. A lumped-parameter electro-thermal model for cylindrical batteries. *Journal of Power Sources*, 2014. 257: 1–11.
105. Gholizadeh, Mehdi, and Farzad R. Salmasi. Estimation of state of charge,unknown nonlinearities, and state of health of a lithium-ion batterybased on a comprehensive unobservable model. *IEEE Transactions on Industrial Electronics*, 2013. 61(3): 1335–1344.
106. Bian, Xiaolei, Longcheng Liu, Jinying Yan, Zhi Zou, and Ruikai Zhao. An open circuitvoltage-based model for state-of-health estimation of lithium-ion bat-teries: Model development and validation. *Journal of Power Sources*, 2020. 448: 227401.